Experimental and numerical investigation on the behaviour of square concrete-filled cold-formed double-skin steel stiffened tubular short columns

Zhang, Jun-Hua; Hassanein, Mostafa Fahmi; Cashell, C.A.; Hadzima-Nyarko, Marijana; Xu, Yang; Shao, Yong-Bo

Engineering Structures 303 (2024) 117560

Contents lists available at ScienceDirect

Engineering Structures

journal homepage: www.elsevier.com/locate/engstruct

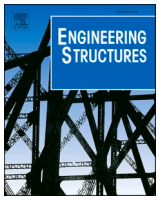

Experimental and numerical investigation on the behaviour of square concrete-filled cold-formed double-skin steel stiffened tubular short columns

Jun-Hua Zhang [a], M.F. Hassanein [a,b,*], K.A. Cashell [c], Marijana Hadzima-Nyarko [d], Yang Xu [e], Yong-Bo Shao [a,e,*]

[a] School of Architecture and Civil Engineering, Xihua University, Chengdu 610039, PR China
[b] Department of Structural Engineering, Faculty of Engineering, Tanta University, Tanta, Egypt
[c] Department of Civil Environmental and Geomatic Engineering, University College London (UCL), London, UK
[d] Faculty of Civil Engineering and Architecture, Josip Juraj Strossmayer University of Osijek, Vladimira Preloga 3, 31000 Osijek, Croatia
[e] School of Civil Engineering and Geomatics, Southwest Petroleum University, Chengdu, Sichuan, 610500, PR China

ARTICLE INFO

Keywords:
Concrete-filled double-skin steel stiffened tube
Axial compression
Experiment analysis
Finite element
Design resistance

ABSTRACT

This paper presents an investigation into a new cold-formed concrete-filled double-skin steel stiffened tubular (CFDSST) column. It consists of concrete filled between two concentrically-located square hollow steel tubes where the outer steel tube is made with four lipped angles of cold-formed plates and lips which can be regarded as longitudinal stiffeners. This new composite column has fewer welds compared to traditional concrete-filled double-skin steel tubular columns with stiffeners. To investigate the axial compression mechanical properties of the column, fifteen short columns were designed and fabricated, including thirteen CFDSST short columns and two concrete-filled stiffened steel tubular (CFSST) columns, for comparison. The specimens were examined under axial compression, and a finite element (FE) model was then developed and validated using the test results. Next, a parametric analysis was carried out to explore the behaviour of the CFDSST columns with different properties. The results show that the ultimate strength of CFDSST columns is significantly affected by the strength of concrete. Finally, different international design methods were assessed to evaluate their applicability and accuracy for these members. In light of the results, a new design formula was proposed for CFDSST columns which accounts for the lateral confining pressure as well as the size effect.

1. Introduction

Nowadays, concrete-filled steel tubular (CFST) columns are widely used in the construction of high-rise buildings and infrastructure due to their various attributes including high strength, good plasticity and excellent fire resistance. However, when CFST columns have a large cross-sectional area, the concrete core greatly increases the weight of column significantly, and may not be fully utilised, whilst also adding to the potential seismic load on the structure. Therefore, the strength-to-weight ratio of composite columns is a key factor in seismic design and always represents a challenge [1–3]. Concrete-filled double-skin steel tubular (CFDST) columns are an excellent solution and have been widely used in practical applications in recent years. CFDST column consists of an inner and outer steel tubes of different sizes which are concentrically located one inside the other, with concrete cast into the sandwich region between the two sections. Since the inner steel tube replaces the central concrete component of CFSTs, the column has increased flexural stiffness, lighter self-weight, as well as superior fire resistance and seismic performance [4–7]. Researchers have studied these members experimentally and numerically with different configurations in recent years [*e.g.* 8–14].

In more recent years, the addition of stiffeners to the outer steel section of CFDST columns has been investigated, creating what are known as concrete-filled double-skin stiffened steel tubular (CFDSST) columns. These can improve the behaviour of composite columns [15–17], since the stiffeners effectively delay local buckling of the outer steel tube. The typical section types of CFDSST columns are shown in

* Corresponding authors at: School of Architecture and Civil Engineering, Xihua University, Chengdu 610039, PR China
E-mail addresses: junhua_zhang2022@163.com (J.-H. Zhang), mostafa.fahmi@f-eng.tanta.edu.eg (M.F. Hassanein), k.cashell@ucl.ac.uk (K.A. Cashell), mhadzimanyarko@gmail.com (M. Hadzima-Nyarko), swpuYX@163.com (Y. Xu), ybshao@swpu.edu.cn (Y.-B. Shao).

https://doi.org/10.1016/j.engstruct.2024.117560
Received 24 November 2023; Received in revised form 22 December 2023; Accepted 21 January 2024
Available online 1 February 2024

Nomenclature

B_o	Width of outer steel tube.
B_i	Width of inner steel tube.
w	Width of the subpanel plate.
t_o	Thickness of the outer steel tube.
t_i	Thickness of the inner steel tube.
t_s	Thickness of the stiffener.
h_s	Height of the longitudinal stiffeners.
L	Height of columns.
$f_{yo\text{-}corner}$	Yield strength of the outer section in the corner.
Δf_{yc}	Increase in yield strength in the steel region.
$f_{yo\text{-}plate}$	Yield strength of the outer section in the flat parts.
f_{yi}	Yield strength of the inner steel tube.
f_{yo}	Yield strength of the outer steel tube.
f_{ys}	Yield strength of the stiffeners.
f_y	Yield strength of steel tube.
f_u	Ultimate tensile strength of steel tube.
f_{cu}	Concrete cube compressive strength.
f_{ck}	Characteristic design strength of concrete.
f_c	Concrete compressive strength.
f_r	Residual stress of confined concrete.
f_{yd}	Yield strength of the structural steel.
f_{cd}	Cylinder compressive strength of concrete.
f_{sd}	Yield strength of reinforcing steel.
f_{cc}	Confined concrete strength.
f_{rp}	Lateral confining pressure on the concrete.
$E_{so\text{-}corner}$	Elastic modulus of the outer section in the corner.
$E_{so\text{-}plate}$	Elastic modulus of the outer section in the flat parts.
E_{si}	Elastic modulus of the inner section.
E_c	Elastic modulus of concrete.
A_c	Cross-sectional areas of concrete.
A_{si}	Cross-sectional areas of inner steel tube.
A_{ss}	Cross-sectional areas of stiffeners.
A_{so}	Cross-sectional areas of outer steel tube.
$A_{sy,eff}$	Effective cross-sectional area of outer steel tube.
A_a	Cross-sectional areas of the structural steel section.
A_s	Cross-sectional areas of reinforcement.
$N_{ul,Exp}$	Ultimate resistance obtained by experiments.
$N_{ul,FE}$	Ultimate resistance obtained by finite element model.
N_s	Total resistance of the section.
$N_{ul,EC4}$	Ultimate resistance of the CFDSST column obtained by EC4 [26].
$N_{ul,BS5400}$	Ultimate resistance of the CFDSST column obtained by BS4500 [27].
$N_{ul,DBJ}$	Ultimate resistance of the CFDSST column obtained by DBJ/T 13–15-2010 [28].
$N_{ul,prop}$	Ultimate resistance of the CFDSST column proposed by author.
$\varepsilon_{85\%}$	Axial strain corresponding to 0.85*N*ul,Exp in the descending branch of the axial load *versus* axial strain response.
$\varepsilon_{75\%}$	Axial strain corresponding to 0.75*N*ul,Exp in the ascending branch of the axial load *versus* axial strain response.
ρ	Reduction factor for plate buckling.
σ	Engineering stress.
σ_{true}	True stress.
ε	Engineering strain.
ε_{true}	True strain.
r	Inner radius of the outer steel tube.
ξ_c	Confinement factor.
e	Flow potential eccentricity.
ψ	Dilation angle.
ν	Viscosity parameter.
K_c	Second stress invariant on the tensile meridian to that on the compressive meridian.
f_{b0}/f_c	Ratio of the compressive strength under biaxial loading to uniaxial compressive strength.
χ	Hollow ratio.
γ_c	Strength reduction factor for the compressive strength that accounts for the size effect of the column.

Fig. 1. Liang et al. [18] studied four types of square CFDSST columns as shown in Fig. 1(a-d). The outer steel tubes were formed by welding two "L-shape" steel parts and the stiffeners were pre-welded to the inner sides of "L-shape" panels. The test results indicated that the ductility of the CFDSST columns was improved due to the presence of stiffeners, but the axial ultimate strength of the four types of CFDSST columns decreased due to the reduction of the effective area of inner concrete. Ding et al. [19] proposed a new type of CFDSST columns by welding steel tubes with "T-shaped" plates and using stiffeners to connect the inner and outer steel tubes. However, the corner of steel tube was prone to cracking due to the defects caused by welding. It was found that stiffeners can delay local buckling of the tube and change its mode and stress path. In addition, Zhang and Chen [20] and Dabaon et al. [21,22] proposed fabricating stiffened composite columns by welding four lipped angles of cold-formed plates. The lips can be regarded as longitudinal stiffeners for the columns. The research results showed that these columns effectively avoided cracking of the outer steel tube at the corners. Wang et al. [23–25] improved this column type further by

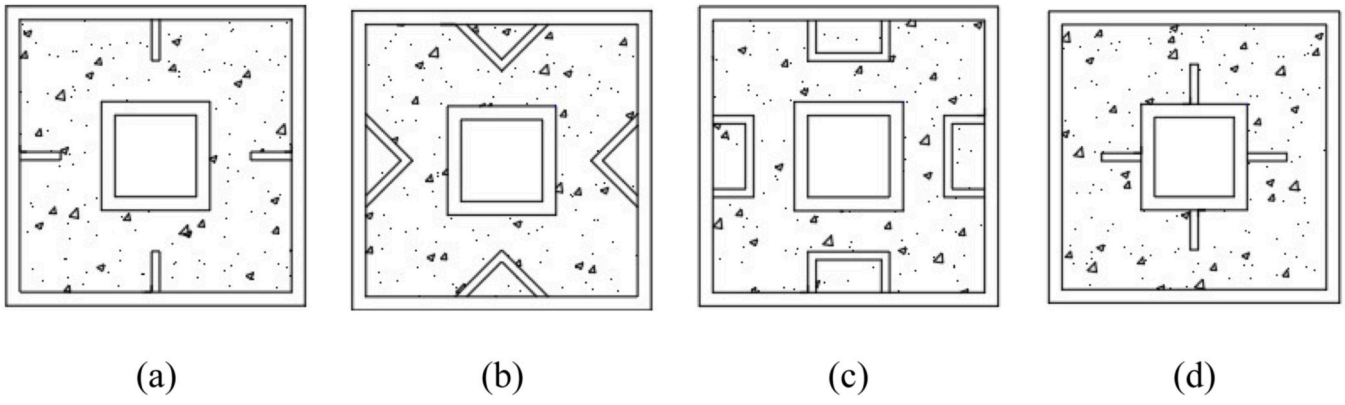

Fig. 1. Different types of CFDSST columns.

introducing the concrete-filled double-skin steel tubular (CFDSST) columns, with the main aim of increasing the strength-to-weight ratio of the column. Up until now, only Wang et al. [23–25] carried out experimental and numerical investigations on the behaviour of CFDSST columns fabricated by welding four lipped angles of cold-formed plates to form the outer steel tube and circular steel tube as inner tube, and this data is only available in Chinese. Their research results showed that the formed CFDSST columns exhibit excellent performance and the stiffeners effectively delay the buckling of the outer tube and no cracking occurs at the welds. However, it is clear that performance information on CFDSST columns is very limited, and no data on the behaviour of CFDSST columns made using square hollow sections, with the outer section fabricated by welding four lipped angles of cold-formed plates, is available in the literature. Therefore, these members are investigated in the current paper.

The paper proceeds with a description of thirteen tests which were conducted on CFDSST short columns with different properties under axial compression, as well as two concrete-filled stiffened steel tubular (CFSST) columns which were also examined for comparison. The different variables examined in the test programme include concrete strength f_c, width-to-thickness ratio of the outer square steel tube B_o/t_o, width-to-thickness ratio of the inner square steel tube B_i/t_i and hollow ratio χ. A finite element (FE) model was also developed and its accuracy and reliability were validated by comparison with test results. This was then employed to conduct a parametric analysis to study the influence of different parameters on the behaviour of CFDSST columns. Finally, the design resistances calculated using international specifications including Eurocode 4 Part 1–1 [26], BS5400 [27] and DBJ/T 13–15-2010 [28] were compared with the experimentally-obtained resistances. A prediction model was established to calculate the ultimate bearing capacity of CFDSST short columns under axial compressive load. Overall, the current paper fills existing knowledge gaps by studying the performance of cold-formed CFDSST short columns with SHS inner and outer tubes under axial compression and provides a useful reference and important performance data for the application of CFDSST columns in civil engineering.

2. Experimental programme

2.1. Design and fabrication of specimens

A total of fifteen short columns were prepared and tested, including thirteen CFDSST short columns and two CFSST columns. The cross-section of the CFDSST columns is presented in Fig. 2(a) and a view of the CFSST columns is shown in Fig. 2(b). The geometric and material properties of the test specimens are given in Table 1, where column labels starting with "S" and "SS" refer to CFSST columns and CFDSST columns, respectively. The next number (either 160 or 200) refers to the width of the outer steel tube and the last number (1−7) represents the serial number of the CFDSST columns. The height of the longitudinal stiffeners is given as h_s in the table whilst f_{cu} is the concrete cube compressive strength. To avoid overall buckling of the columns, the height (L) of columns was taken as three times the total width (B_o) of the outer steel tube. The height of the stiffeners was taken as 30 mm for the current test specimens, which was designed to satisfy the rigidity requirement in Eq. (1) proposed by Tao et al. [29]:

$$I_s = 3.1 \times 10^{-4} \left(\frac{w}{t_s}\right) \frac{f_{yo}}{280} t_s^4 \quad (1)$$

where w presents the width of the subpanel plate and it is to be taken as $0.5B_o$-$2t_o$; and t_s is the thickness of the stiffener and it is to be taken as $2t_o$ for the CFDSST columns tested in this paper.

The CFDSST columns consisted of two endplates, four lipped angles welded to create the outer tube, a welded square steel inner tube and the concrete, as shown in Fig. 2. The fabrication process of the outer steel tube is shown in Fig. 3. In the specimen preparation, both the inner and outer steel tubes were welded to the bottom endplate, which had a thickness of 20 mm. The concrete was then filled into the gap between the two steel sections and compacted using a vibrator. After 14 days of curing, a layer of high-strength mortar was applied to the top of each specimen to ensure the flushness of the top surface. Twenty eight days after concrete pouring, another end plate of 20 mm thickness was welded to the top end of each column. The fabrication process of CFDSST columns is presented in Fig. 4.

2.2. Material properties

2.2.1. Concrete

The mix design for the concrete is presented in Table 2, where w/c represents the water-to-cement ratio. As observed in the table, four different concrete mixes were designed with target compressive strengths of 40, 50, 60 and 70 MPa, respectively. The actual compressive strengths of the concrete were determined by testing standard cube specimens with a side of 150 mm. At least three cubes were crushes for each mix, and the average compressive strength values f_{cu} are presented in Table 2.

2.2.2. Steel

The outer steel tube and inner steel tube were fabricated from Q235B steel grade and the endplate was fabricated from Q355A steel grade. Standard tensile coupon tests were carried out to examine the mechanical properties of the steel used in the specimens. In order to consider the effect of cold bending of the outer steel tube, an additional tensile coupon test specimen was cut from the corner of the steel plate after bending. The locations of tensile coupon test specimens are shown in Fig. 5. The dimensions of tensile test specimens conformed to American Standard ASTMA370–2017 [30] and the details of the tensile coupons are shown in Fig. 6. The tensile test specimens were tested according to international [30] and nations specifications [31] in a 1000 kN universal testing machine. A calibrated extensometer with a

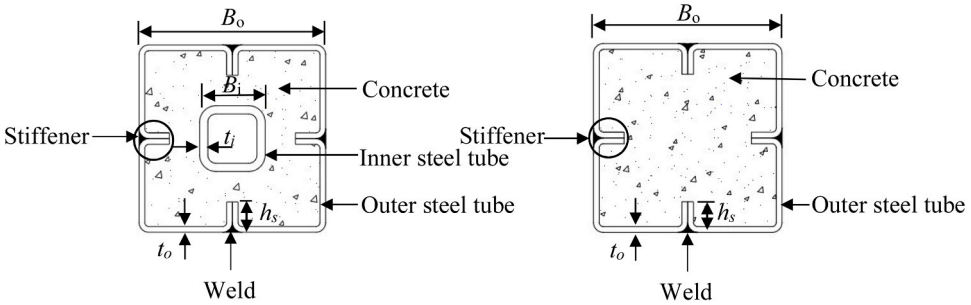

Fig. 2. Details of the CFDSST and CFSST specimens examined in the current programme.

Table 1
Details of specimens and results.

Group	Specimens	B_o (mm)	t_o (mm)	h_s (mm)	B_i (mm)	t_i (mm)	f_{cu} (MPa)	*DI*	*SI*	$N_{ul,Exp}$ (kN)	$N_{ul,FE}$ (kN)	$N_{ul,FE}/N_{ul,Exp}$
CFSST	S-160	160	1.9	30	-	-	74.3	2.98	0.95	1894.6	2016.1	1.06
	S-200	200	1.9	30	-	-	74.3	2.65	1.10	3226.7	3119.5	0.97
CFDSST	SS-160-1	160	1.9	30	50	2.76	50.2	2.83	1.14	1727.6	1637.1	0.95
	SS-160-2	160	1.9	30	50	2.83	53.7	2.46	1.19	1884.4	1712.6	0.91
	SS-160-3	160	1.9	30	50	2.83	87.6	1.85	1.25	2858.8	2638.6	0.92
	SS-160-4	160	1.9	30	60	2.74	50.2	3.41	1.14	1722.9	1613.0	0.94
	SS-160-5	160	2.7	30	50	2.79	50.2	2.70	1.05	1916.4	1881.0	0.98
	SS-160-6	160	2.7	30	60	2.75	50.2	3.99	1.05	1905.4	1843.2	0.97
CFDSST	SS-200-1	200	1.9	30	50	2.83	50.2	2.99	1.10	2338.4	2327.4	1.00
	SS-200-2	200	1.9	30	50	2.78	53.7	2.41	1.02	2303.0	2319.9	1.01
	SS-200-3	200	1.9	30	50	2.84	74.3	2.17	1.03	3037.4	3138.1	1.03
	SS-200-4	200	1.9	30	50	2.80	87.6	2.13	0.97	3312.6	3601.8	1.09
	SS-200-5	200	1.9	30	60	2.77	50.2	2.64	1.11	2359.0	2247.3	0.95
	SS-200-6	200	2.7	30	50	2.76	50.2	3.99	0.96	2407.8	2619.3	1.09
	SS-200-7	200	2.7	30	60	2.73	50.2	2.51	1.07	2655.5	2571.4	0.97
Mean												**0.99**
COV												**0.056**

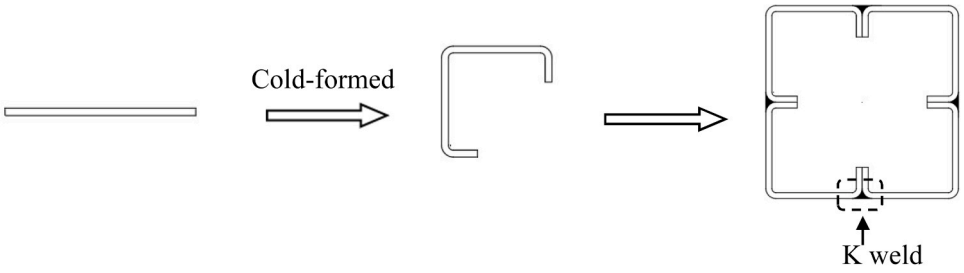

Fig. 3. Process diagram of the outer steel tube.

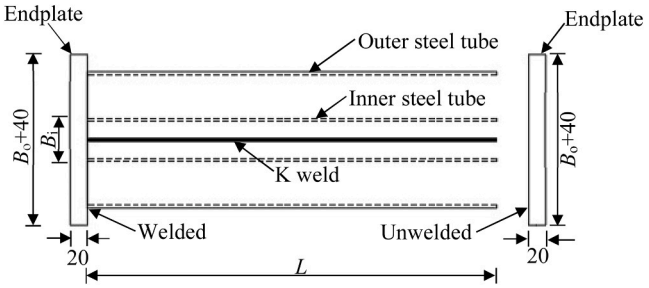

Fig. 4. Fabrication process of CFDSST columns (all units are in mm).

Table 2
Mix design and properties of the concrete.

Concrete mix	Unit	C40	C50	C60	C70
Cement	kg/m^3	454.55	408.16	526	386.84
Coarse aggregate	kg/m^3	1047.27	1075.10	1002.00	1014.76
Fine aggregate	kg/m^3	698.18	716.73	725.00	676.51
Water	kg/m^3	200.00	200.00	163.00	155.40
w/c	%	0.44	0.49	0.31	0.28
Fly ash	kg/m^3	-	-	-	122.10
Silica fume	kg/m^3	-	-	-	44.40
Water reducer	kg/m^3	-	-	1.052	1.665
Concrete cube strength (f_{cu})	MPa	50.2	53.7	74.3	87.6

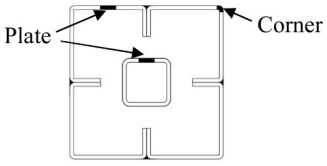

Fig. 5. Location of tensile coupon test specimen.

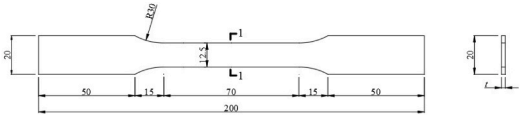

(a) For the plate region of the outer section

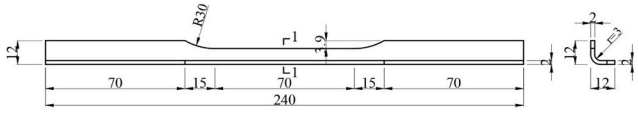

(b) For corner region of the outer section with a normal thickness of 2 mm

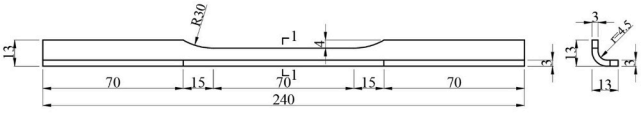

(c) For corner region of the outer section with a normal thickness of 3 mm

Fig. 6. Dimensions of the tensile test coupons.

gauge length of 50 mm was used to measure the longitudinal strain until fracture. The yield strength and the elastic modulus of the steel tubes are presented in Table 3, where $f_{yo\text{-}corner}$, $f_{yo\text{-}plate}$ and f_{yi} are the yield strengths of the outer section in the corner, the outer section in the flat parts and the inner section, respectively. $E_{so\text{-}corner}$, $E_{so\text{-}plate}$ and E_{si} are the corresponding elastic modulus values.

2.3. Testing procedure

A 10,000 kN capacity hydraulic testing machine was utilised to apply the axial compressive force to the test specimens, as depicted in Fig. 7. The instrumentation and measuring devices used in the tests are presented in Fig. 7. The locations of the dial gauges on the specimens can also be seen as Fig. 7. All of the columns were positioned in the testing machine to ensure perfect alignment and verticality. To avoid localized crushing of the concrete in the loading regions, champing devices were used at both ends of the columns as recommended by Rohola et al. [32]. The ultimate axial resistance of the test specimens ($N_{ul,Exp}$) was predicted before testing using finite element (FE) analysis (as described later in this paper). During the testing, until the applied axial load reached 50% of the predicted load (*i.e.* $0.5N_{ul,FE}$, where $N_{ul,FE}$ is the ultimate load predicted by the FE model), load control was adopted with a load interval of $0.25N_{ul,FE}$ and a loading rate of 5 N/s, and at each level the load was held for about 2 min. After that, displacement control was adopted with a displacement rate of 0.5 mm/min until the axial shortening of the column corresponded to an applied load which was approximately 60% of the ultimate load capacity in the descending part of the curve.

3. Test results and discussion

3.1. Failure modes of specimens

Fig. 8 presents a selection of photographs of CFDSST columns after testing. Overall, the observations during the response of the specimens can be divided into three different stages. Firstly, in the elastic stage, there were no obvious changes observed in the outer tubes. Then, in the second stage, there was audible evidence of concrete crushing before the ultimate load was reached, but there was still no obvious deformation in the specimens. Thereafter, in the final stage (*i.e.* post-peak loading stage), the outer steel tubes began to demonstrate some deformations and more significant crushing of the concrete developed. It was also noted that the local outward buckling of the outer steel tube developed rapidly after the ultimate load was reached. As evident in Fig. 8, all of the CFDSST columns failed by local outward buckling of the outer steel tubes. There was no evidence of steel fracture in the corner regions, ensuring good deformation capacity of the CFDSST columns. The local buckling locations mostly occurred between the column end and the mid-height section and generally not in the same cross-section, avoiding the total loss of bearing capacity at that cross-section. Additionally, the failure modes of CFDSST columns were observed to be similar to the CFSST columns. Fig. 9 shows the failure modes of the concrete and the inner steel tube after testing, which were observed by removing some of the outer steel and the infill concrete. With reference to Fig. 9(a), it is observed that the concrete has undergone significant crushing. This is due to the relatively weak confinement which exists after the outer thin-walled steel tube has locally buckled. The levels of deformation of the inner steel tubes are presented in Fig. 9(b) and it is observed that the inner steel tube has buckled inward.

Table 3
Material properties of steel.

Steel tube	t_o (mm)	$f_{yo\text{-}corner}$ (MPa)	$E_{so\text{-}corner}$ (GPa)	$f_{yo\text{-}plate}$ (MPa)	$E_{so\text{-}plate}$ (GPa)
Outer	1.9	363.7	203.4	293.9	203.2
	2.7	420.8	201.6	336.6	200.4
Steel tube	B_i (mm)	f_{yi} (MPa)	E_{si}(GPa)		
Inner	50	331	202.1		
	60	335.2	201.7		

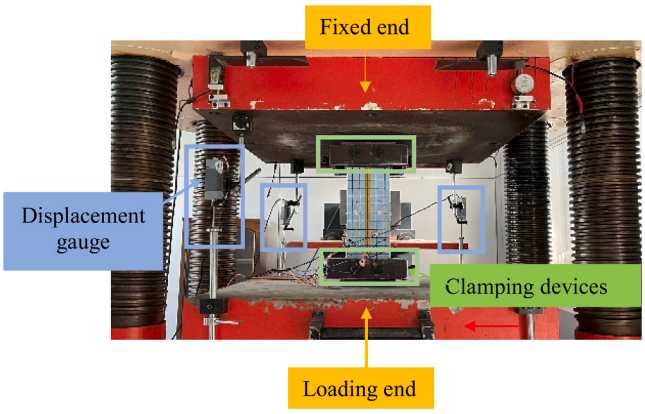

Fig. 7. Test setup and clamping device.

3.2. Axial load versus deflection

The axial load *versus* deflection responses for all test specimens are presented in Fig. 10. From the results presented, it is observed that the overall shape is quite similar for all specimens, and can generally be divided into three key stages, *i.e.* the elastic stage, the elastic-plastic stage and then the descending branch of the response (post-peak loading stage). The initial stiffness in the elastic range is very similar for all specimens, with the exception of column SS-160–6 in Fig. 10(a) which had a slightly stiffer response. This is likely to be owing to experimental conditions during that test and the relatively thicker outer steel tube employed in this member, compared with the other specimens. Again, in Fig. 10(a), it is observed that specimen SS-160–3 had the highest load carrying capacity, owing to the concrete strength in this column. With regard to the post-peak loading stage, it is observed that the CFDSST columns had greater load resistance than the CFSST columns. This is due to the presence of the inner steel tube. With regard to specimens with B_o of 200 mm (presented in Fig. 10(b)), the same result can be expected because the curve appears with a significant downward slope (without reaching a turning point representing the start point of the residual strength of the column) before early termination of S-200 specimen test.

3.3. Ultimate load and ductility index (DI)

Table 1 presents the highest ultimate load $N_{ul,Exp}$ achieved in the experiments, and it is observed that the highest capacity was obtained for the test specimen SS-200–4. This was the column with the largest cross-section of those examined, and also contained the highest strength concrete. The table also includes the ductility index *DI* for each of these specimens, determined in accordance with the expression given in Eq. (2) [15]:

$$DI = \frac{\varepsilon_{85\%}}{\varepsilon_{75\%}/0.75} \tag{2}$$

where $\varepsilon_{85\%}$ is the axial strain corresponding to $0.85N_{ul,Exp}$ in the descending branch of the axial load *versus* axial strain response and $\varepsilon_{75\%}$ is the axial strain corresponding to $0.75N_{ul,Exp}$ in the ascending branch of the same curve. In addition to the values given in Table 1, Fig. 11 also presents a graphical representation of the *DI* data. By comparing SS-160–1, SS-160–2 and SS-160–3, it is observed that when the strength of the infill concrete was increased from C40 to C60 and C70, $N_{ul,Exp}$ increased from 1727.6 kN to 1884.4 kN and 2858.8 kN representing

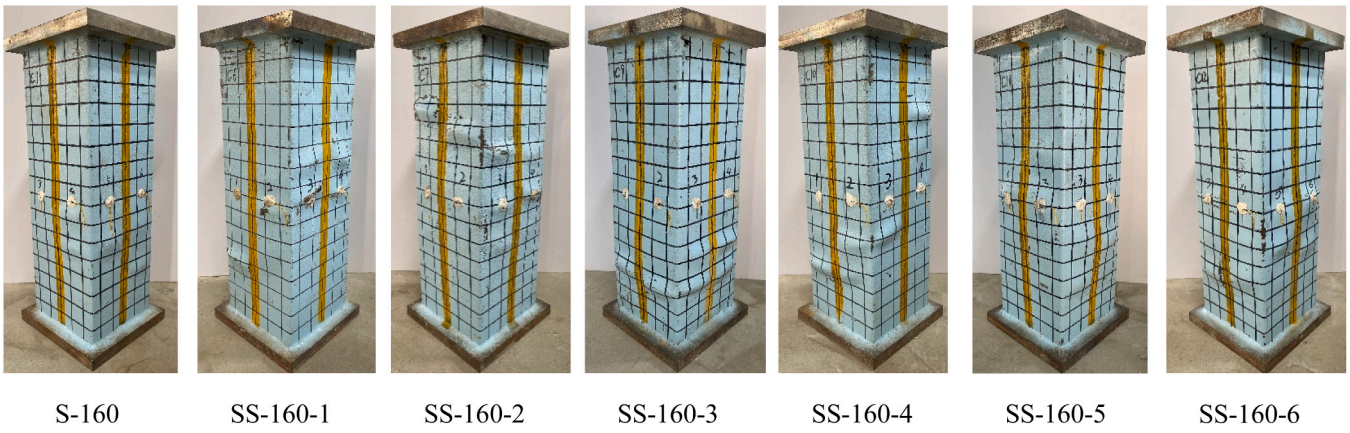

Fig. 8. Typical specimens after testing.

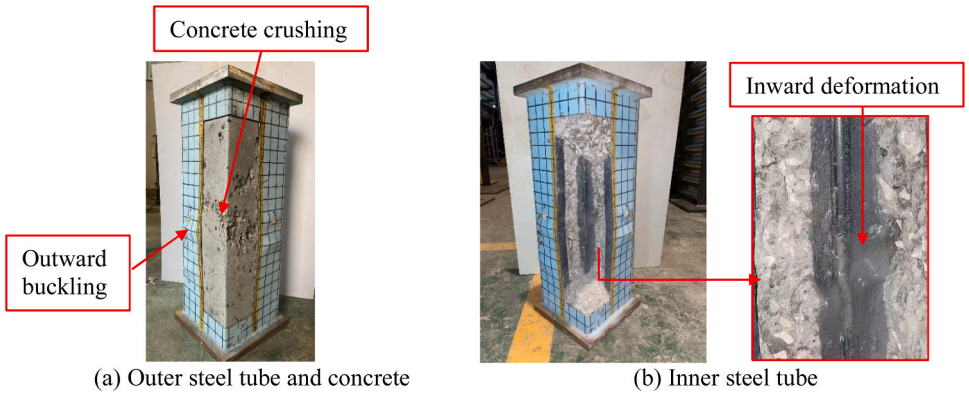

Fig. 9. Failure modes of tube and concrete of a typical specimen.

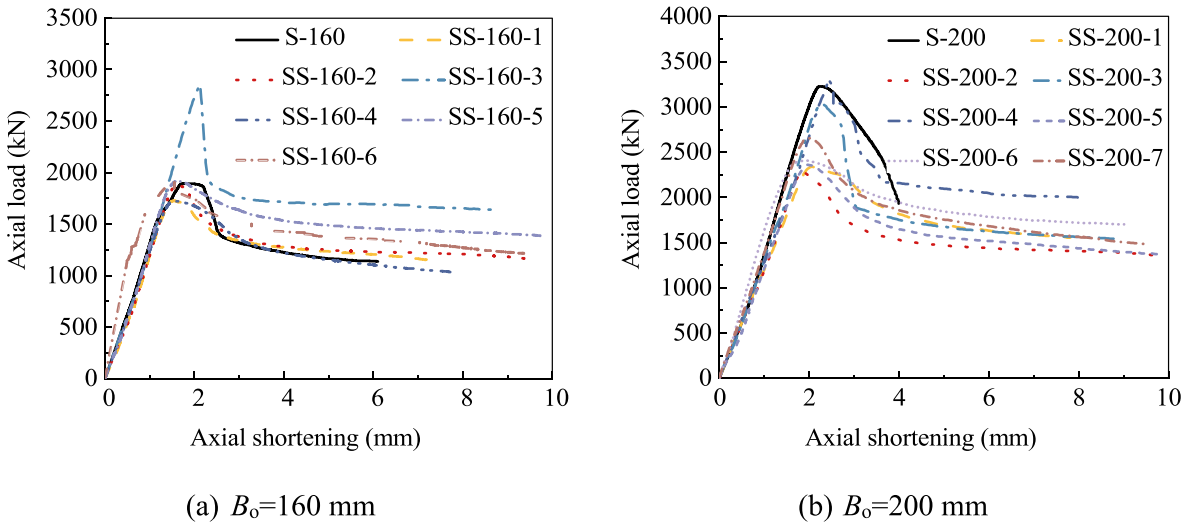

Fig. 10. Axial load-displacement responses for the test specimens.

increases of 9.08% and 65.48%, respectively. On the other hand, for these same specimens, the *DI* decreased from 2.83 to 2.46 and 1.85 representing reductions of 13.07% and 34.53%, respectively. This clearly demonstrates that although employing higher strength concrete can enhance the axial compressive bearing capacity, it is accompanied by a reduction in ductility.

By comparing SS-160–1 and SS-160–4, it is evident that when the hollow ratio (defined herein as B_i/B_o) increased from 0.313 to 0.375, there was little effect on the axial compressive bearing capacity, but the *DI* increased from 2.83 to 3.41 (*i.e.* 20.49%). The *DI* was increased for members with relatively higher hollow ratio owing to the greater cross-sectional area of steel provided. For members SS-160–4 and SS-160–6, it was observed that when the width-to-thickness (B_o/t_o) ratio of the outer tube decreased from 84.21 to 59.26, $N_{ul,Exp}$ increased from 1722.9 kN to 1905.4 kN representing an increase of 10.59%, while the *DI* increased from 3.41 to 3.99 (*i.e.* 17.0%). Therefore, the axial compressive capacity

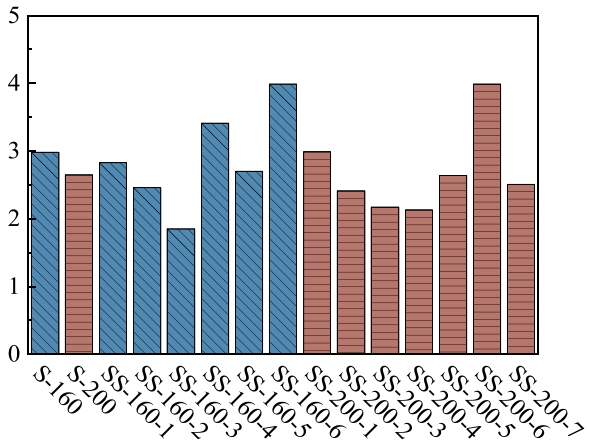

Fig. 11. Comparison of *DI* for test specimens.

and the ductility index of CFDSST columns tend to increase with a reduction of B_o/t_o ratio owing to the increased stiffness of these cross-sections.

3.4. Strength index (SI)

The strength index *SI* is a property which was developed to illustrate the relative influence of the combined resistance of the component elements in CFDST columns [33], and it is determined in accordance with the expression given in Eq. (3) for CFDSST columns:

$$SI = \frac{N_{ul}}{N_s} \tag{3}$$

where N_{ul} represents the ultimate resistance of specimens obtained by experimental testing ($N_{ul,Exp}$) or through finite element analysis ($N_{ul,FE}$) as given in Table 1. N_s refers to the total resistance of the section, and is calculated as the summation of the resistance of each of the component elements, as given in Eq. (4):

$$N_s = A_{sy,eff} f_{yo} + A_{ss} f_{ys} + A_{si} f_{yi} + A_c f_c \tag{4}$$

where f_{yo}, f_{ys} and f_{yi} are the yield strengths of the outer steel tube, the stiffeners and the inner steel tube, respectively, and f_c is the concrete compressive strength of the concrete. The relationship between the concrete compressive strength (f_c) and the concrete cube compressive strength (f_{cu}) is defined as given in Eq. (5):

$$f_c = \left[0.76 + 0.2\log_{10}\left(\frac{f_{cu}}{19.6}\right)\right] f_{cu} \tag{5}$$

A_c, A_{si} and A_{ss} are the cross-sectional areas of the concrete, the inner steel tube and the steel stiffeners, respectively. For the outer steel tube, the effective area method proposed in Eurocode 3 [34] is used to calculate the effective cross-sectional area ($A_{sy,eff}$), to account for the increased propensity of these elements to buckle locally. $A_{sy,eff}$ is calculated as:

$$A_{sy,eff} = \rho A_{so} \tag{6}$$

where A_{so} is the cross-sectional area of the steel section and ρ is the reduction factor for plate buckling, as defined in Eq. (7):

$$\rho = \begin{cases} 1.0 & \bar{\lambda}_p \le 0.673 \\ \dfrac{\bar{\lambda}_p - 0.055(3+\psi)}{\bar{\lambda}_p^2} & \bar{\lambda}_p > 0.673, \ \text{where}(3+\psi) \ge 0 \end{cases} \tag{7}$$

where ψ is the stress ratio and is taken as 1.00 for symmetrical cross-sections, while $\bar{\lambda}_p$is defined as:

$$\bar{\lambda}_p = \sqrt{\frac{f_y}{\sigma_{cr}}} = \frac{B_o/2t_o}{28.3\varepsilon\sqrt{k_\sigma}} \tag{8}$$

where ε is taken as $\sqrt{235/f_y}$and k_σ is taken as 4 when $\psi = 1$.

The *SI* value for each specimen determined using Eq. (3) is given in Table 1. For the thirteen CFDSST columns, it is observed that the *SI* values ranged between 0.96 and 1.25. Note that members whose SI values exceed unity are those for whom the combined action contributed positively to the load-bearing capacity of the member. From Table 1, it is clearly observed that the *SI* value of specimens with a width of 160 mm was generally higher than that of specimens with a width of 200 mm. The highest *SI* value was obtained for specimen SS-160–3 which had the highest strength concrete infill of the B_o= 160 mm members. On the other hand, the lowest *SI* value was obtained from specimen SS-200–6, which was almost identical to SS-200–4 apart from the concrete strength, indicating that this is a very influential parameter for the strength index.

4. Finite element analysis

It was clear during the experimental programme that the geometric and material parameters of the columns were very influential to the overall behaviour, including load-carrying capacity and ductility. In order to investigate a wider range of parameters than was possible in the physical testing programme, a finite element (FE) model was developed using the ABAQUS software [35] and validated against the experimental results.

4.1. Development of the FE model

4.1.1. Initial model conditions

A FE model was developed for each of the test specimens discussed in the current paper, using the geometric and material properties given in Table 1, and schematic views of the model are presented in Fig. 12. In all cases, the model comprises two rigid plates at the member ends, the infill concrete, as well as the inner and outer steel tubes. The steel tubes were modelled using four-node shell elements with reduced integration (*i.e.* the S4R elements in the ABAQUS software), whilst 8-node brick elements with three translation degrees of freedom at each node (C3D8R) were employed for the infill concrete and the endplates. A mesh sensitivity study was conducted in order to optimise computation efficiency as well as accuracy of the results. As a result of this study, the element sizes across the cross-section were selected as 12 mm and 15 mm for specimens with B_o equal to 160 mm and 200 mm, respectively, whilst the corresponding element sizes in the axial direction were 24 mm and 30 mm for the same column sizes. The end conditions of the columns are shown in Fig. 12, where it is shown that the bottom end of the columns were fully fixed, with no movement permitted for any of the degrees of freedom (*i.e.* $U_1 = U_2 = U_3 = UR_1 = UR_2 = UR_3 = 0$, where U_1,U_2 and U_3 are translations in the X, Y and Z, directions respectively, and UR_1, UR_2 and UR_3 are the rotational degrees of freedom about the X, Y and Z axes, respectively). On the other hand, at the top of the columns, all degrees of freedom were again restrained, apart from U_3, which is translation in the Z direction, corresponding to axial displacements. There were two reference points defined at the centre of each endplate and the axial displacement was applied through the top reference point. Therefore, the ultimate loads and axial load *versus* displacement responses of the specimens were taken at this point.

The four lipped angles were connected using the 'tie' constraint between the contact faces of the stiffeners. Both endplates were set as rigid bodies and were effectively tied to the steel tubes. A 'surface to surface contact' was defined at the interfaces between the concrete and the steel (*i.e.* the concrete and the end plates, as well as the concrete and the steel tubes), including a 'hard contact' in the normal direction and a 'penalty

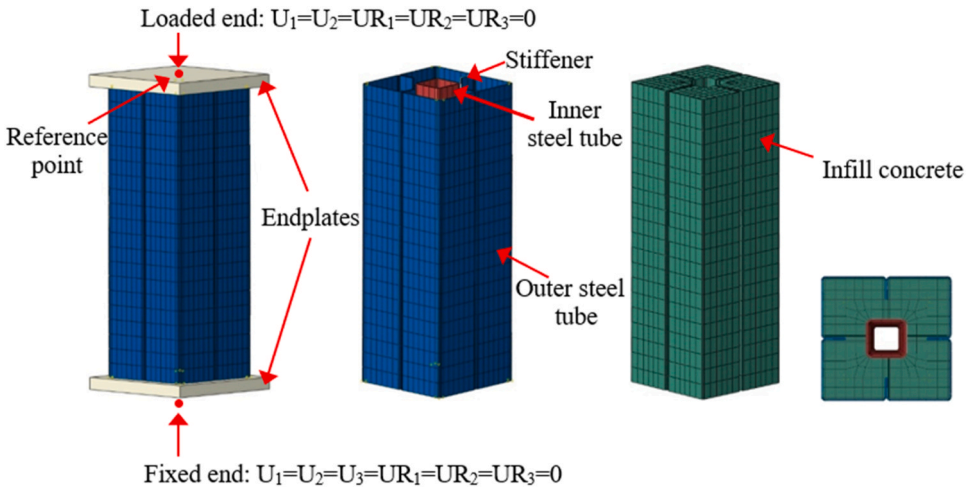

Fig. 12. Typical FE model with meshing scheme, load and boundary conditions.

constraint algorithm' to simulate the tangential behaviour. The friction coefficient between the steel and the concrete was selected as 0.6, in accordance with the guidance elsewhere for similar elements [36].

4.1.2. Initial imperfections

Geometric imperfections develop in steel sections during their production, as well as if welding is used and they can be quite influential to the material behaviour. However, it has been shown that geometric imperfections generally have a negligible effect on the performance of composite columns [37,38]. Tao et al. [38] found that initial imperfections had no significant effect on the behaviour of stiffened thin-walled CFSST columns, mainly because the concrete plays a much more significant role than the steel in terms of load-capacity. Therefore, initial geometric imperfections were not included in the FE simulation, to reduce the computational effort. On the other hand, the enhanced strength which develops in the corner regions of cold-formed tubes during the fabrication process, were accounted for, as discussed in the following section. While residual stresses affects the behaviour of bare steel tubes, they have negligible effect on composite columns as found by Tao et al. [17]. Accordingly, they have been ignored in the current FE modelling.

4.1.3. Material modelling

The steel was modelled using an elastic-perfectly plastic material model, as shown in Fig. 13(a); this rather simple model was considered as a useful method for square steel tube in which the resistance of steel tubes is dominated by local buckling [37]. In the FE model, the engineering stress (σ) and strain (ε) were converted into true stress (σ_{true}) and strain (ε_{true}), as required in the ABAQUS model, using Eqs. (9–10), respectively:

$$\sigma_{true} = \sigma \times (1+\varepsilon) \tag{9}$$

$$\varepsilon_{true} = \ln(1+\varepsilon) - \frac{\sigma_{true}}{E} \tag{10}$$

As stated before, the additional strength which develops in cold-formed steel sections in the corner regions during fabrication were also accounted for the in the model, as illustrated in Fig. 14. The increase in yield strength in the steel region (Δf_{yc}) was determined using Eq. (11) according to the guidance proposed elsewhere [39]:

$$\Delta f_{yc} = 0.6\left[\frac{B_c}{(r/t)^m} - 1.0\right] f_y \tag{11}$$

where r is the inner radius of the corner of the outer steel tube (Fig. 14) and is taken as $1.5t_o$ in the current paper; B_c and m are coefficients related to the ratio of f_u to f_y determined in accordance with the expression given in Eqs. (12–13); and f_u is the ultimate tensile strength of the steel tube and determined using Eq. (14).

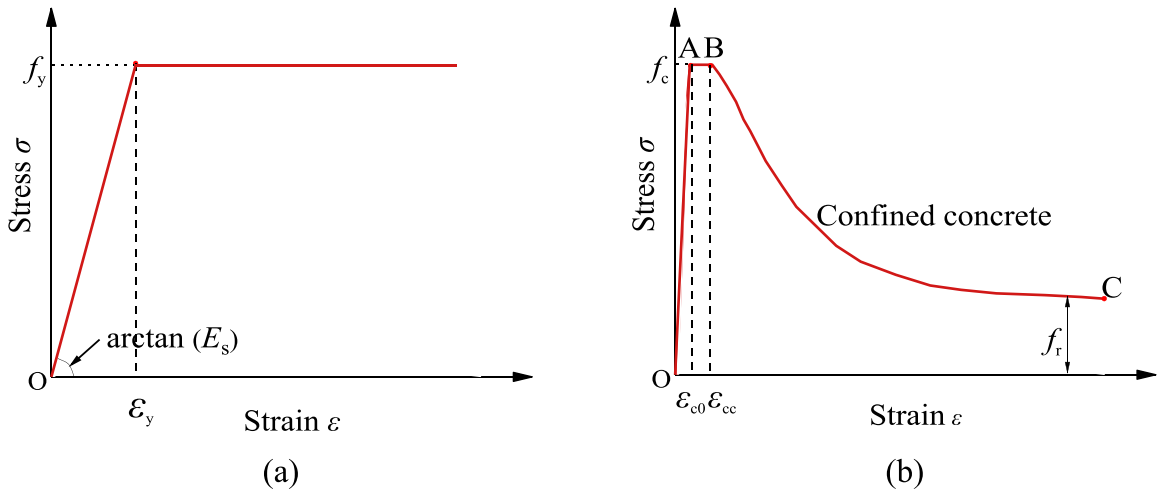

Fig. 13. Material models for (a) steel and (b) infill concrete.

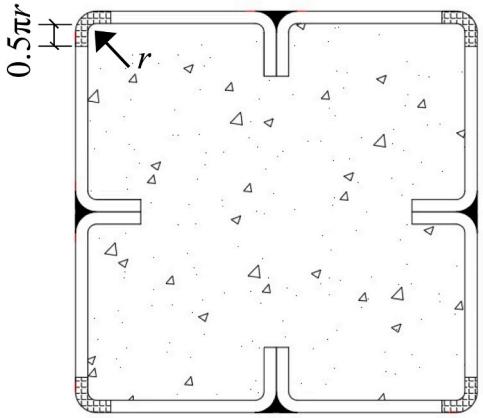

Fig. 14. The location of strengthening effect caused by cold-forming developed in the corner regions.

$$B_c = 3.69\left(\frac{f_u}{f_y}\right) - 0.819\left(\frac{f_u}{f_y}\right)^2 - 1.79 \tag{12}$$

$$m = 0.192\left(\frac{f_u}{f_y}\right) - 0.068 \tag{13}$$

$$f_u = \left[1 + 1.4 \times \left(\frac{130}{f_y}\right)\right] f_y \tag{14}$$

For the infill concrete, the concrete damaged plasticity (CDP) model proposed by Tao et al. [40] was employed to simulate the behaviour using the material model for confined concrete presented in Fig. 13(b) and given in Eq. (15):

$$\sigma = \begin{cases} \dfrac{AX + BX^2}{1 + (A-2)X + (B+1)X^2} f_c & 0 < \varepsilon \le \varepsilon_{c0} \\ f_c & \varepsilon_{c0} < \varepsilon \le \varepsilon_{cc} \\ f_r + \left(f_c - f_r\right)\exp\left[-\left(\dfrac{\varepsilon - \varepsilon_{cc}}{\alpha}\right)^{\beta}\right] & \varepsilon \ge \varepsilon_{cc} \end{cases} \tag{15}$$

In these expressions, $X = \varepsilon/\varepsilon_{c0}$, $A = (E_c\varepsilon_{c0})/f_c$, $B = ((A-1)^2/0.55) - 1.0$ and E_c is taken as $4700\sqrt{f_c}$, and these terms are defined as shown in Fig. 13(b). The residual stress f_r was taken as 0.1 f_c. The parameter α was determined in accordance with the expression given in Eq. (16) and β was taken as 0.92.

$$\alpha = 0.005 + 0.0075\xi_c \tag{16}$$

The strain values at point A (ε_{c0}) and at point B (ε_{cc}) were determined as given in Eqs. 17 and 17, respectively.

$$\varepsilon_{c0} = 0.00076 + \sqrt{\left(0.626 f_c - 4.33\right) \times 10^{-7}} \tag{17}$$

$$\frac{\varepsilon_{cc}}{\varepsilon_{c0}} = e^k,$$
$$k = \left(2.9224 - 0.00367 f_c^{'}\right)\left(\frac{f_B}{f_c}\right)^{0.3124 + 0.002 f_c} \tag{18}$$

where f_B was proposed by Tao et al. [40] based on a regression analysis, and as expressed as:

$$f_B = \frac{0.25 \cdot \left(1 + 0.027 f_y\right) \cdot e^{-0.02\sqrt{B^2 + D^2}}}{1 + 1.6 e^{-10} \cdot (f_c)^{4.8}} \tag{19}$$

The confinement factor ξ_c is a crucial parameter for composite columns, and is expressed as:

$$\xi_c = \frac{A_s f_y}{A_c f_{ck}} \tag{20}$$

where A_s and A_c are the cross-sectional areas of the steel tube and infill concrete, respectively, and f_y and f_{ck} are the characteristic design strengths of the two component materials, respectively, and f_{ck} was taken as 0.67 f_{cu}. To simplify the calculation, the stiffeners were not considered when determining A_s and A_c as suggested by other researchers [31]. The other parameters required in the CDP model include the flow potential eccentricity (e), the dilation angle (ψ) and the viscosity parameter (ν) and these were taken as 0.1, 40° and 0.0001, respectively. The other parameters including the second stress invariant on the tensile meridian to that on the compressive meridian (K_c) [41], the modulus of elasticity (E_c) [40] and ratio of the compressive strength under biaxial loading to uniaxial compressive strength (f_{b0}/f_c) [40] are defined in accordance with Eqs. (21–23), respectively:

$$K_c = \frac{5.5}{5 + 2(f_c)^{0.075}} \tag{21}$$

$$E_c = 4700\sqrt{f_c} \tag{22}$$

$$f_{b0}/f_c = 1.5(f_c)^{-0.075} \tag{23}$$

4.2. Validation of the FE model

The test data presented previously in this paper are employed in the current section to validate the numerical model, and there are three different performance indicators employed to assess the accuracy of the model (i) a comparison of the axial load *versus* axial shortening responses, (ii) a comparison of the ultimate loads $N_{ul,FE}$ and $N_{ul,Exp}$, and (iii) a comparison of the failure modes. Firstly, Fig. 15 presents a comparison of the axial load *versus* axial shortening results from both the experiments and the FE models, with only four representations shown for brevity considerations. It is observed that the overall shape of the responses is very similar, and the numerical model is clearly able to provide a good depiction of the general response. The initial stiffness and the ultimate loads are also well represented, whilst the descending branch in the post-peak range, are also very well matched. As expected for this type of comparison, there are some minor differences between the numerical and experimental results and these are attributed to differences between the real and idealised material properties, as well as slight errors which may have developed in the support and loading conditions during the tests.

Table 1 provides the ultimate load predictions from the FE model $N_{ul,FE}$ together with those from the tests $N_{ul,Exp}$ as well as the $N_{ul,FE}/N_{ul,Exp}$ ratio. It is observed that the mean $N_{ul,FE}/N_{ul,Exp}$ ratio and coefficient of variation (COV) values are 0.99 and 0.056, respectively, which demonstrates the accuracy of the FE model. For the failure modes, Fig. 16 presents a comparison of the deformed shapes from the FE model and the corresponding experiment for a selection of columns, which represent the full range of failure modes observed. It is observed that the model is capable of capturing the key failure modes which occurred in the tests, including buckling of the outer and inner steel tubes as shown in Fig. 9. Overall, the observations and comparisons presented herein indicate that the FE model is capable of providing an excellent depiction of the real response of CFDSST columns including the axial load *versus* axial shorting responses (Fig. 15), the ultimate capacities (Table 1), and the failure modes (Fig. 16).

5. Comparison of CFDSST and CFSST columns

In this section, the behaviour of concrete-filled double-skin steel stiffened tubular (CFDSST) columns is compared with that of concrete-filled stiffened steel (CFSST) columns, thus examining the influence of

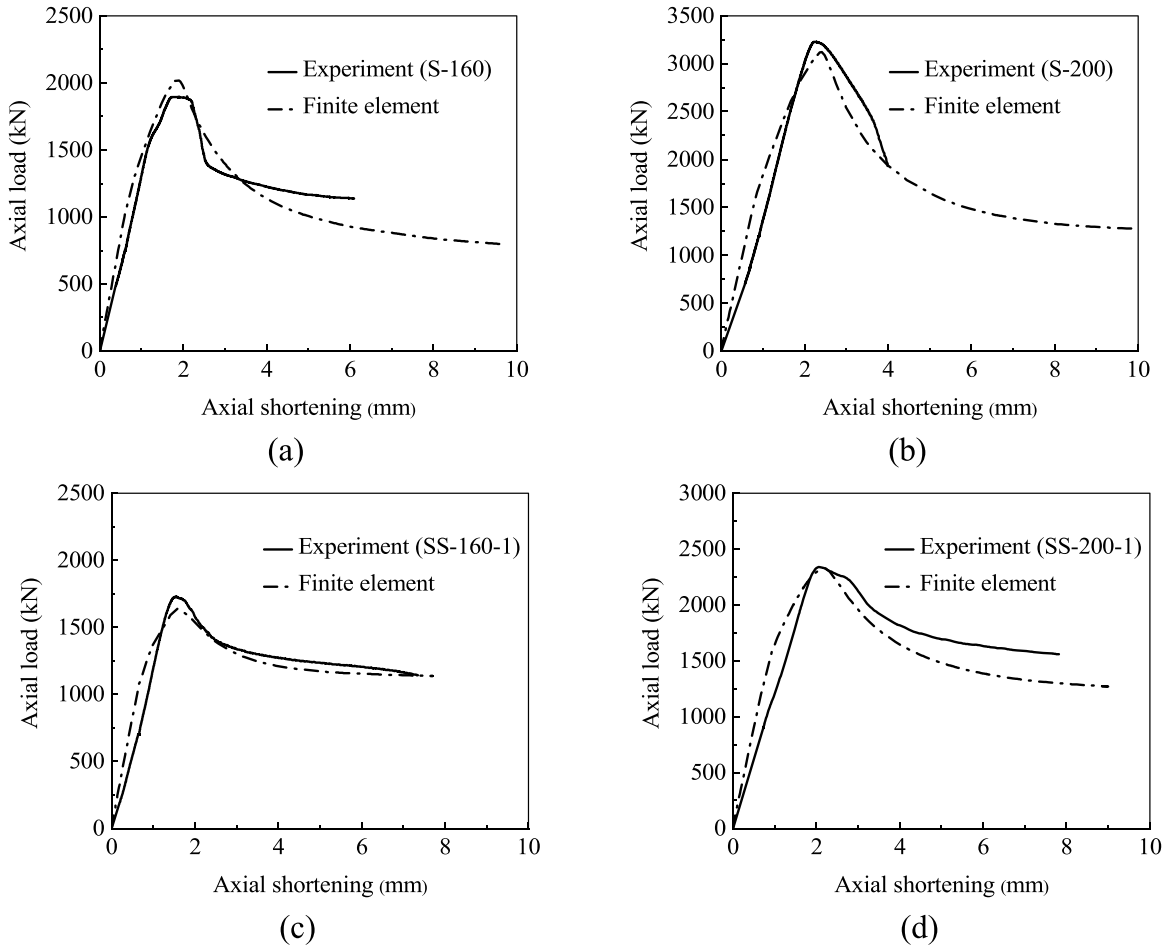

Fig. 15. Comparison of numerical and experimental load *versus* axial shortening curves.

the inner steel tube and reduced concrete infill material in the double-skin members on the behaviour. Fig. 17(a) presents the axial load *versus* axial shorting responses for S-200 and SS-200–3, which were identical in terms of outer tube dimensions and concrete strength. It is shown that the structural performances, including the ultimate resistances, are almost identical although the CFSST contains 5.6% more concrete than the CFDSST, which in turn, contains the additional thin-walled inner tube. In this case, it is clear that the contributions made by the difference in concrete areas between the CFDSST and CFSST members, and the contribution made by the inner steel tube in the CFDSST, are very similar in terms of their influence on the structural response. It is also noteworthy that as concrete has a much greater density than steel, and the difference in concrete volumes between CFSSTs and CFDSSTs can be significant, the strength to weight ratio for CFDSSTs is typically very favourable compared with CFSSTs. CFDSSTs also offer greater flexural rigidity owing to the presence of the inner steel tube.

On the other hand, the composite action between the steel tubes and sandwiched concrete can be evaluated by drawing the load *versus* $\varepsilon_h/\varepsilon_l$ ratio relationships for steel tubes, as presented in Fig. 17(b).ε_h is the transverse strain at the mid-height of the columns andε_l is the corresponding longitudinal strain at the same point. When the $\varepsilon_h/\varepsilon_l$ ratio becomes greater than 0.3, the concrete becomes confined. As can be noticed, the outer tubes of columns S-200 and SS-200–3 show generally the same behaviour within the entire loading range, where the confinement effect ($\varepsilon_h/\varepsilon_l$>0.3) of the concrete starts before reaching the ultimate load. For case of the inner tube of SS-200–3, the inner tube confines effectively the concrete at the same load as the outer tubes, although it does so slightly from the start of loading.

With regard to the concrete stress, Fig. 17(c) presents the stress contour of the sandwiched concrete at three load levels; 75%$N_{ul,FE}$ in ascending branch (before the initiation of concrete confinement), $N_{ul,FE}$ and 75%$N_{ul,FE}$ in descending branch. From the stress contour, it can be seen that CFDSST columns are more effective in confining central concrete after the ultimate load compared to CFSST columns.

6. Parametric analysis

A series of parametric studies were performed on CFDSST columns to fully investigate their behaviour and to evaluate the relative influence of different parameters on their ultimate performance. Previous research showed that the yield strength of the inner tube has a relatively insignificant effect on the behaviour of composite columns [42], so this value f_{yi} was fixed at 235 MPa. The variables examined in the parametric analysis include the yield steel strength of the outer tube f_{yo}, the concrete strength f_c, the depth of the stiffeners h_s, the width to thickness ratio of the outer steel tube B_o/t_o and the hollow ratio B_i/B_o. A total of 127 models were simulated, and they were divided into four different groups according to different B_o values. The values of $N_{ul,FE}$ obtained from the parametric studies are presented in Table 4, along with the details of the study. The results are divided into 4 groups (G1 to G4), depending on B_o.

6.1. Yield strength of the outer tube f_{yo}

Fig. 18 presents the axial load *versus* axial shortening responses for a range of scenarios, to illustrate the influence of f_{yo}. This study was conducted for a range of B_o/t_o ratios, and it was observed that the key

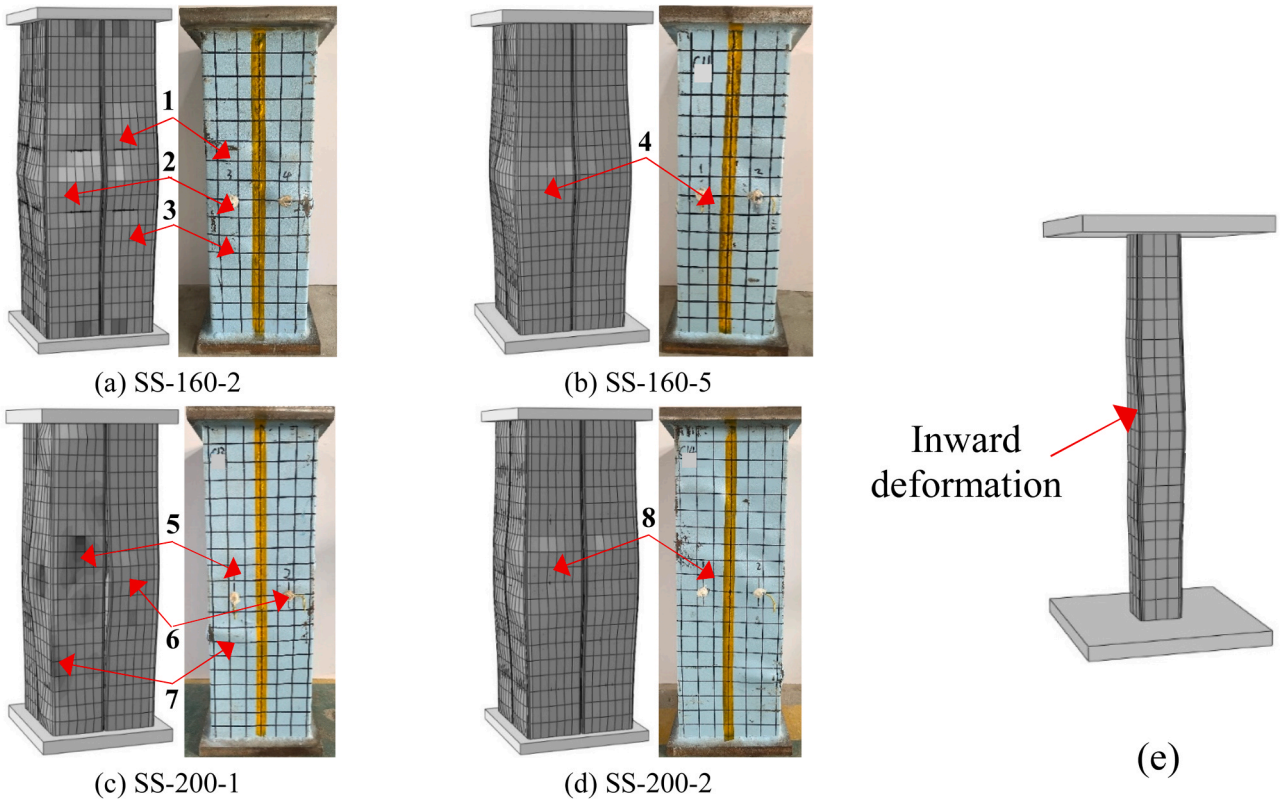

Fig. 16. Comparison of numerical and experimental deformed shapes for a range of typical specimens.

findings were identical for all of the value examined; therefore, for brevity, the results for B_o/t_o= 72 are presented herein for illustration. It is clear that increasing f_{yo} has the effect of improving the axial compressive capacity and the post-peak bearing capacity of CFDSST columns. The influence of f_{yo} on the ductility of CFDSST columns is shown in Fig. 19(a) where it is observed that the *DI* tends to increase for higher f_{yo} values and this trend is more pronounced as B_o/t_o ratio reduces.

6.2. Concrete strength

A range of different concrete strengths were examined for the infill material, varying between 30 and 60 MPa. The influence of this property on the axial load *versus* axial displacement response is shown in Fig. 20. As in the previous section, it is noteworthy that this analysis was conducted for columns with a range of B_o/t_o ratios, and the observations were identical. Therefore, for brevity, the results for B_o/t_o= 72 are presented herein to demonstrate the key findings. It is evident that increasing the strength of the concrete can significantly improve the axial compressive capacity of the columns. The effect of the concrete strength on the ductility of CFDSST columns is shown in Fig. 19(b). It is observed that the ductility of CFDSST columns reduces with increasing concrete strength. Additionally, it is noteworthy concrete strength has a greater effect on the ductility compared with the steel yield strength.

Table 5 also presents the $\Delta N_{ul,FE}/\Delta f_{yo}$ and $\Delta N_{ul,FE}/\Delta f_c$ ratios, which is a measure that was proposed by Ayough et al. [35] to evaluate the efficiency of improving the ultimate resistance of CFDSST columns ($\Delta N_{ul,FE}$) by increasing the steel strength of the outer tube Δf_{yo} or the concrete strength (Δf_c). It is observed that $\Delta N_{ul,FE}/\Delta f_{yo}$ is less than 0.40 in all cases whereas $\Delta N_{ul,FE}/\Delta f_c$ varies between 0.5 and 0.8 which indicates that for the range of values examined herein, the increases in concrete strength had a greater influence on the ultimate capacity, compared with using higher steel grades. This is likely to be a function of the relative cross-sectional areas of the two materials in the cross-section, as well as the particular material grades examined.

6.3. B_o/t_o

To illustrate the effect of the width-to-thickness ratio of the outer tube (B_o/t_o) on the resistance of CFDSST columns, the relationship between B_o/t_o and the f_c for CFDSST columns is shown in Fig. 21. The influence of B_o/t_o ratio on the ultimate resistance of CFDSST columns with different concrete strengths, steel yield strengths, stiffener depths and widths of the inner tube is presented. Overall, it is clear that in all cases examined, the ultimate resistance of CFDSST columns reduces with increasing B_o/t_o ratios. This is because increasing the B_o/t_o ratio by reducing the tube thickness, lowers the confining stresses that develop on the concrete. The effect of B_o/t_o ratio on the ductility of CFDSST columns with different concrete strengths is presented in Fig. 22. Here, it is observed that the *DI* values decrease with increasing B_o/t_o ratios irrespective of the concrete infill strength.

6.4. Hollow ratio χ

The hollow ratio χ is an important parameter for double-skin composite columns and is defined herein as B_i/B_o. The relationships between hollow ratio and the capacity and ductility of CFDSST columns are presented in Fig. 23 and Fig. 24, respectively, where χ was varied between 0.227 and 0.457. It is observed that the axial capacity generally reduced for higher values of χ but the influence of χ was relatively limited for the range of specimens examined. On the other hand, with reference to Fig. 24, it is shown that the ductility of CFDSST columns generally increased for columns with higher hollow ratios, especially when $\chi > 0.4$. It is noteworthy that columns with relatively high χ values, have lower self-weight and material usage requirements for the same B_o value, and therefore can provide an efficient structural solution.

(a) axial load-shorting of CFDSST and CFSST columns

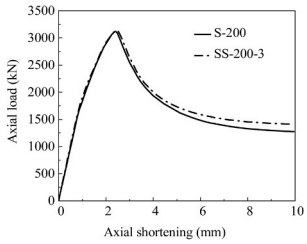

(b) Load- $\varepsilon_h / \varepsilon_l$ ratio relationships of the steel tubes

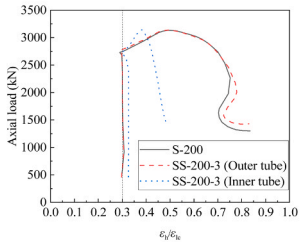

(c) Stress contour

S-200 SS-200-3

At 75%$N_{ul,FE}$ in ascending branch

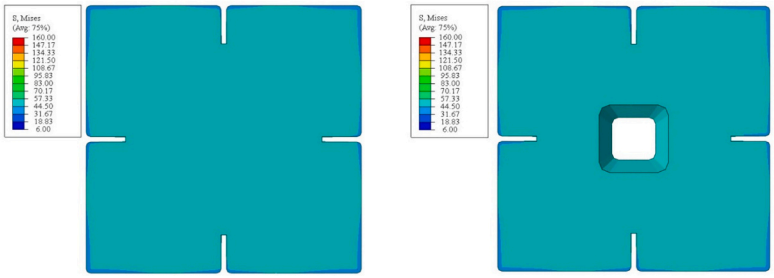

At $N_{ul,FE}$

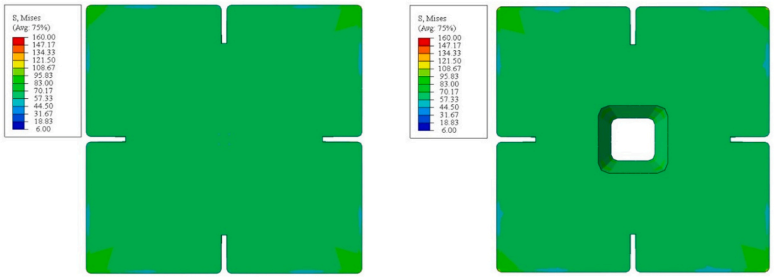

At 75%$N_{ul,FE}$ in descending branch

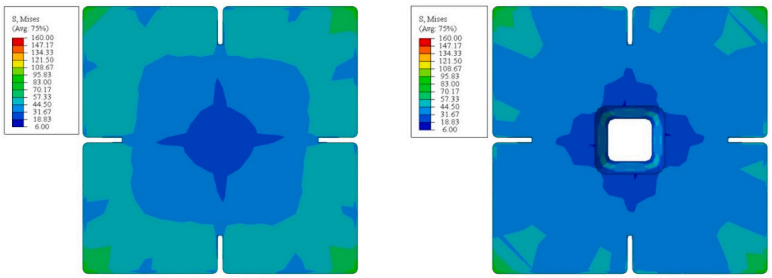

Fig. 17. Comparison between CFDSST and CFSST columns.

Table 4
Details and results from the parametric study on CFDSST columns.

Groups	specimens	B_o (mm)	t_o (mm)	B_o/t_o	B_i (mm)	t_i (mm)	χ	f_{yo} (MPa)	f_{yc} (MPa)	f_{yi} (MPa)	f_c (MPa)	h_s (mm)	$N_{ul,FE}$ (kN)	*DI*	*SI*
G1	C1	180	2	90	40	2	0.222	235	330	235	30	30	1434.6	2.33	1.06
	C2	180	2	90	40	2	0.222	235	330	235	40	30	1714.2	1.96	1.05
	C3	180	2	90	40	2	0.222	235	330	235	50	30	2009.8	1.74	1.04
	C4	180	2	90	40	2	0.222	235	330	235	60	30	2303.1	1.61	1.04
	C5	180	2	90	40	2	0.222	275	356	235	30	30	1487.1	2.56	1.06
	C6	180	2	90	40	2	0.222	355	416	235	30	30	1631.9	2.65	1.09
	C7	180	2	90	40	2	0.222	420	470	235	30	30	1762.2	2.50	1.12
	C8	180	2	90	40	2	0.222	235	330	235	30	40	1464.0	2.36	1.06
	C9	180	2	90	40	2	0.222	235	330	235	30	50	1486.6	2.49	1.05
	C10	180	2	90	40	2	0.222	235	330	235	30	60	1518.7	2.48	1.05
	C11	180	2	90	60	2	0.333	235	330	235	30	30	1402.1	2.41	1.06
	C12	180	2	90	70	2	0.389	235	330	235	30	30	1362.3	2.51	1.04
	C13	180	2	90	80	2	0.444	235	330	235	30	30	1320.5	2.60	1.03
	C14	180	2.5	72	40	2	0.222	235	330	235	30	30	1531.7	2.59	1.04
	C15	180	2.5	72	40	2	0.222	235	330	235	40	30	1815.9	2.09	1.03
	C16	180	2.5	72	40	2	0.222	235	330	235	50	30	2101.3	1.82	1.03
	C17	180	2.5	72	40	2	0.222	235	330	235	60	30	2388.3	1.67	1.03
	C18	180	2.5	72	40	2	0.222	275	356	235	30	30	1617.9	2.73	1.04
	C19	180	2.5	72	40	2	0.222	355	416	235	30	30	1789.5	2.95	1.05
	C20	180	2.5	72	40	2	0.222	420	470	235	30	30	1948.7	3.00	1.08
	C21	180	2.5	72	40	2	0.222	235	330	235	30	40	1558.4	2.70	1.03
	C22	180	2.5	72	40	2	0.222	235	330	235	30	50	1592.4	2.84	1.02
	C23	180	2.5	72	40	2	0.222	235	330	235	30	60	1631.8	2.96	1.02
	C24	180	2.5	72	60	2	0.333	235	330	235	30	30	1492.8	2.78	1.03
	C25	180	2.5	72	70	2	0.389	235	330	235	30	30	1459.4	2.83	1.02
	C26	180	2.5	72	80	2	0.444	235	330	235	30	30	1417.5	3.04	1.01
	C27	180	3	60	40	2	0.222	235	330	235	30	30	1627.4	2.93	1.04
	C28	180	3	60	40	2	0.222	235	330	235	40	30	1911.1	2.27	1.04
	C29	180	3	60	40	2	0.222	235	330	235	50	30	2193.3	1.93	1.03
	C30	180	3	60	40	2	0.222	235	330	235	60	30	2438.4	1.82	1.01
	C31	180	3	60	40	2	0.222	275	356	235	30	30	1736.2	3.16	1.04
	C32	180	3	60	40	2	0.222	355	416	235	30	30	1933.6	3.56	1.02
	C33	180	3	60	40	2	0.222	420	470	235	30	30	2123.3	3.65	1.03
	C34	180	3	60	40	2	0.222	235	330	235	30	40	1674.7	3.05	1.04
	C35	180	3	60	40	2	0.222	235	330	235	30	50	1716.3	3.21	1.03
	C36	180	3	60	40	2	0.222	235	330	235	30	60	1756.6	3.36	1.03
	C37	180	3	60	60	2	0.333	235	330	235	30	30	1591.2	3.11	1.03
	C38	180	3	60	70	2	0.389	235	330	235	30	30	1563.3	3.21	1.03
	C39	180	3	60	80	2	0.444	235	330	235	30	30	1513.8	3.56	1.01
G2	C40	240	2	120	40	2	0.167	235	330	235	30	30	2265.1	1.88	1.07
	C41	240	2	120	40	2	0.167	235	330	235	40	30	2793.2	1.69	1.05
	C42	240	2	120	40	2	0.167	235	330	235	50	30	3334.0	1.56	1.04
	C43	240	2	120	40	2	0.167	235	330	235	60	30	3884.4	1.47	1.04
	C44	240	2	120	40	2	0.167	275	356	235	30	30	2348.5	1.97	1.08
	C45	240	2	120	40	2	0.167	355	416	235	30	30	2560.0	2.04	1.13
	C46	240	2	120	40	2	0.167	420	470	235	30	30	2649.8	1.99	1.13
	C47	240	2	120	40	2	0.167	235	330	235	30	40	2270.7	1.95	1.05
	C48	240	2	120	40	2	0.167	235	330	235	30	50	2327.8	1.95	1.06
	C49	240	2	120	40	2	0.167	235	330	235	30	60	2358.7	1.97	1.06
	C50	240	2	120	60	2	0.250	235	330	235	30	30	2240.9	1.90	1.07
	C51	240	2	120	70	2	0.292	235	330	235	30	30	2219.2	1.93	1.07
	C52	240	2	120	80	2	0.333	235	330	235	30	30	2172.3	1.96	1.06
	C53	240	2.5	96	40	2	0.167	235	330	235	30	30	2449.3	2.12	1.07
	C54	240	2.5	96	40	2	0.167	235	330	235	40	30	2979.3	1.80	1.06
	C55	240	2.5	96	40	2	0.167	235	330	235	50	30	3507.6	1.64	1.05
	C56	240	2.5	96	40	2	0.167	235	330	235	60	30	4010.1	1.55	1.04
	C57	240	2.5	96	40	2	0.167	275	356	235	30	30	2560.1	2.24	1.09
	C58	240	2.5	96	40	2	0.167	355	416	235	30	30	2787.4	2.33	1.11
	C59	240	2.5	96	40	2	0.167	420	470	235	30	30	2949.0	2.21	1.13
	C60	240	2.5	96	40	2	0.167	235	330	235	30	40	2468.3	2.20	1.06
	C61	240	2.5	96	40	2	0.167	235	330	235	30	50	2516.7	2.20	1.06
	C62	240	2.5	96	40	2	0.167	235	330	235	30	60	2541.1	2.30	1.06
	C63	240	2.5	96	60	2	0.250	235	330	235	30	30	2418.8	2.16	1.07
	C64	240	2.5	96	70	2	0.292	235	330	235	30	30	2396.1	2.19	1.07
	C65	240	3	80	40	2	0.167	235	330	235	30	30	2558.6	2.26	1.04
	C66	240	3	80	40	2	0.167	235	330	235	40	30	3083.0	1.88	1.04
	C67	240	3	80	40	2	0.167	235	330	235	50	30	3605.8	1.68	1.03
	C68	240	3	80	40	2	0.167	235	330	235	60	30	4127.7	1.57	1.03
	C69	240	3	80	40	2	0.167	275	356	235	30	30	2691.8	2.40	1.05
	C70	240	3	80	40	2	0.167	355	416	235	30	30	2960.8	2.55	1.08
	C71	240	3	80	40	2	0.167	420	470	235	30	30	3185.3	2.58	1.10
	C72	240	3	80	40	2	0.167	235	330	235	30	40	2602.4	2.31	1.04
	C73	240	3	80	40	2	0.167	235	330	235	30	50	2644.9	2.34	1.04

(*continued on next page*)

Table 4 (*continued*)

Groups	specimens	B_o (mm)	t_o (mm)	B_o/t_o	B_i (mm)	t_i (mm)	χ	f_{yo} (MPa)	f_{yc} (MPa)	f_{yi} (MPa)	f_c (MPa)	h_s (mm)	$N_{ul,FE}$ (kN)	*DI*	*SI*
	C74	240	3	80	40	2	0.167	235	330	235	30	60	2693.4	2.37	1.04
	C75	240	3	80	60	2	0.250	235	330	235	30	30	2532.2	2.30	1.04
	C76	240	3	80	70	2	0.292	235	330	235	30	30	2506.7	2.33	1.04
	C77	240	3	80	80	2	0.333	235	330	235	30	30	2463.3	2.37	1.03
G3	C78	300	2	150	40	2	0.133	235	330	235	30	30	3288.8	1.84	1.06
	C79	300	2	150	40	2	0.133	235	330	235	40	30	3999.7	1.70	1.01
	C80	300	2	150	40	2	0.133	235	330	235	50	30	4982.8	1.46	1.04
	C81	300	2	150	40	2	0.133	235	330	235	60	30	5814.5	1.40	1.03
	C82	300	2	150	40	2	0.133	275	356	235	30	30	3440.8	1.88	1.09
	C83	300	2	150	40	2	0.133	355	416	235	30	30	3580.5	1.96	1.10
	C84	300	2	150	40	2	0.133	235	470	235	30	40	3362.2	2.18	1.07
	C85	300	2	150	40	2	0.133	235	330	235	30	50	3397.3	1.85	1.07
	C86	300	2	150	40	2	0.133	235	330	235	30	60	3436.4	1.86	1.07
	C87	300	2	150	60	2	0.200	235	330	235	30	30	3303.6	1.81	1.07
	C88	300	2	150	70	2	0.233	235	330	235	30	30	3255.4	1.83	1.07
	C89	300	2	150	80	2	0.267	235	330	235	30	30	3201.6	1.79	1.06
	C90	300	2.5	120	40	2	0.133	235	330	235	30	30	3392.9	1.78	1.04
	C91	300	2.5	120	40	2	0.133	235	330	235	40	30	4272.4	1.33	1.04
	C92	300	2.5	120	40	2	0.133	235	330	235	50	30	5130.8	1.51	1.03
	C93	300	2.5	120	40	2	0.133	235	330	235	60	30	5985.3	1.44	1.03
	C94	300	2.5	120	40	2	0.133	275	356	235	30	30	3486.6	1.83	1.04
	C95	300	2.5	120	40	2	0.133	355	416	235	30	30	3633.9	2.01	1.04
	C96	300	2.5	120	40	2	0.133	420	470	235	30	30	3742.6	1.81	1.04
	C97	300	2.5	120	40	2	0.133	235	330	235	30	50	3597.2	1.96	1.07
	C98	300	2.5	120	40	2	0.133	235	330	235	30	60	3652.3	1.96	1.08
	C99	300	2.5	120	60	2	0.200	235	330	235	30	30	3503.2	1.91	1.08
	C100	300	2.5	120	70	2	0.233	235	330	235	30	30	3480.7	1.92	1.08
	C101	300	2.5	120	80	2	0.267	235	330	235	30	30	3455.9	1.94	1.08
	C102	300	3	100	40	2	0.133	235	330	235	30	30	3711.2	2.03	1.07
	C103	300	3	100	40	2	0.133	235	330	235	40	30	4552.3	1.74	1.06
	C104	300	3	100	40	2	0.133	235	330	235	50	30	5385.9	1.59	1.05
	C105	300	3	100	40	2	0.133	235	330	235	60	30	6223.9	1.50	1.04
	C106	300	3	100	40	2	0.133	275	356	235	30	30	3873.6	2.09	1.09
	C107	300	3	100	40	2	0.133	355	416	235	30	30	4200.2	2.18	1.12
	C108	300	3	100	40	2	0.133	420	470	235	30	30	4465.0	2.16	1.14
	C109	300	3	100	40	2	0.133	235	330	235	30	40	3748.5	2.06	1.07
	C110	300	3	100	40	2	0.133	235	330	235	30	50	3808.6	2.08	1.07
	C111	300	3	100	40	2	0.133	235	330	235	30	60	3850.3	2.10	1.07
	C112	300	3	100	60	2	0.200	235	330	235	30	30	3689.3	2.04	1.07
	C113	300	3	100	70	2	0.233	235	330	235	30	30	3661.9	2.06	1.07
	C114	300	3	100	80	2	0.267	235	330	235	30	30	3636.3	2.07	1.07
G4	C115	600	6	100	180	6	0.300	235	330	235	30	80	14644.5	2.17	1.05
	C116	600	6	100	180	6	0.300	235	330	235	40	80	17683.1	1.46	1.04
	C117	600	6	100	180	6	0.300	235	330	235	50	80	20719.9	1.66	1.03
	C118	600	6	100	180	6	0.300	235	330	235	60	80	23757.8	1.57	1.02
	C119	600	6	100	180	6	0.300	275	356	235	30	80	15298.6	2.23	1.06
	C120	600	6	100	180	6	0.300	355	416	235	30	80	16606.3	2.23	1.09
	C121	600	6	100	180	6	0.300	420	470	235	30	80	17668.9	2.20	1.11
	C122	600	6	100	180	6	0.300	235	330	235	30	90	14742.9	2.18	1.05
	C123	600	6	100	180	6	0.300	235	330	235	30	100	14858.8	2.20	1.05
	C124	600	6	100	180	6	0.300	235	330	235	30	120	15020.5	2.25	1.05
	C125	600	6	100	240	6	0.400	235	330	235	30	80	13854.1	2.25	1.02
	C126	600	6	100	280	6	0.467	235	330	235	30	80	13295.9	2.36	1.01
	C127	600	6	100	320	6	0.533	235	330	235	30	80	12546.2	2.49	0.99

6.5. *Stiffener depth* h_s

The influence of h_s on the resistance and ductility of CFDSST columns was investigated by varying h_s between 30 and 60 mm and the relationships are presented in Fig. 25 and Fig. 26, respectively. It is observed that the load resistance generally increases for h_s higher values, but not significantly, whilst the ductility also improves, irrespectively of B_o/t_o. This indicates that whilst the presence of stiffeners improves both the load-carrying and ductility performance of composite columns, the size of the stiffener does not need to be very high in order to achieve positive results.

7. Design resistances

Currently, there are no design specifications available for CFDSST columns in international design standards. Accordingly, the applicability of the design expressions given in Eurocode 4 [26], BS5400 [27] and DBJ/T 13–15-2010 [28] for CFDSSTs was examined and the results are discussed in the current section. Based on the findings, and the observations for the parametric studies previously presented, a new design model specifically for CFDSST columns is proposed. It is noteworthy that the effective area method as defined in Eurocode 3 [34] was used to determine the area of the stiffened outer steel tubes.

7.1. *Eurocode 4 [26]*

Eurocode 4 contains a design expression to determine the ultimate compression resistance $N_{pl,Rd}$ of CFST composite cross-sections, comprising an outer steel tube, infill concrete and steel reinforcement. The expression is given as:

$$N_{pl,Rd} = A_a f_{yd} + 0.85 A_c f_{cd} + A_s f_{sd} \tag{24}$$

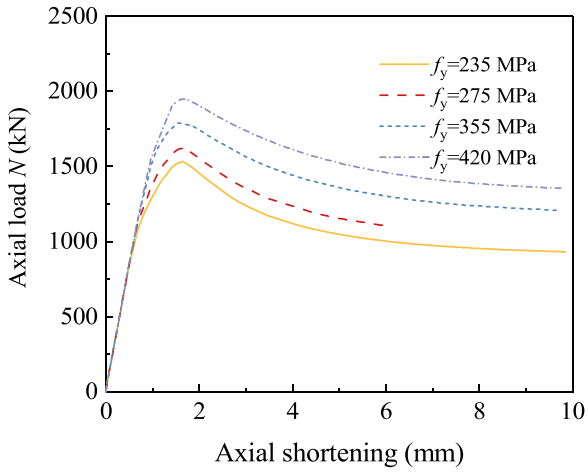

Fig. 18. Influence of steel yield strength of outer tube on the axial load *versus* displacement responses of CFDSST columns with $B_o/t_o = 72$.

where A_a, A_c, A_s are the cross-sectional areas of the structural steel section, concrete and reinforcement, respectively, and f_{yd}, f_{cd}, f_{sd} are the design values for the yield strength of the structural steel, the cylinder compressive strength of the concrete, and the yield strength of reinforcing steel, respectively. In this approach, the confinement effect on the infill concrete is neglected and the concrete compressive strength (f_c) is reduced by 15% to account for long term effects [26]. In order to apply the Eurocode expression for CFDSST columns, the reinforcement is effectively replaced by the contribution of the inner steel section and the stiffeners, resulting in the expression given in Eq. (25):

$$N_{ul,EC4} = A_{sy,eff} f_{yo} + A_{si} f_{yi} + A_{ss} f_{ys} + 0.85 A_c f_c \quad (25)$$

where $N_{ul,EC4}$ is the ultimate capacity of the CFDSST column, $A_{sy,eff}$ is the effective cross-sectional area of the outer steel tube, f_{ys} is the yield strength of the stiffeners, and A_c, A_{si} and A_{ss} are the cross-sectional areas of the infill concrete, inner steel tube and stiffeners, respectively.

7.2. BS5400 [27]

In accordance with BS5400 [27], the compressive resistance of CFDSST columns $N_{ul,BS5400}$ is calculated as:

$$N_{ul,BS5400} = A_{sy,eff} f_{yo} + A_{ss} f_{ys} + A_{si} f_{yi} + 0.675 A_c f_{cu} \quad (26)$$

It is noted that the concrete cube strength (f_{cu}) is employed in this equation and the confinement effect on the concrete which is provided by the outer steel tube is neglected in this approach.

7.3. DBJ/T 13-15-2010 [28]

In this approach [28], and in contrast to Eurocode 4 [26] and BS5400 [27], the effect of confinement on the infill concrete is taken into account using the confinement factor ξ, to determine the overall capacity $N_{ul,DBJ}$. The expression to determine $N_{ul,DBJ}$ is given in Eq. (27) and it is noted that the characteristic compressive strength of the concrete (f_{ck}) is employed, which is taken as $0.67 f_{cu}$:

$$N_{ul,DBJ} = (A_{sy,eff} + A_c)(1.18 + 0.85\xi) f_{ck} + A_{si} f_{yi} + A_{ss} f_{ys} \quad (27)$$

All of the other terms in Eq. (27) are defined elsewhere in this paper.

7.4. New design method

As stated before, the aforementioned design expressions do not currently contain specific design expressions for CFDSST columns, and

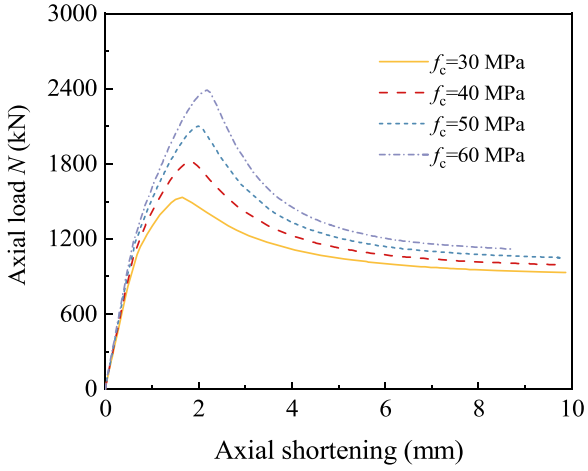

Fig. 20. Effect of infill concrete strength on the axial load *versus* axial displacement responses of CFDSST columns with $B_o/t_o = 72$.

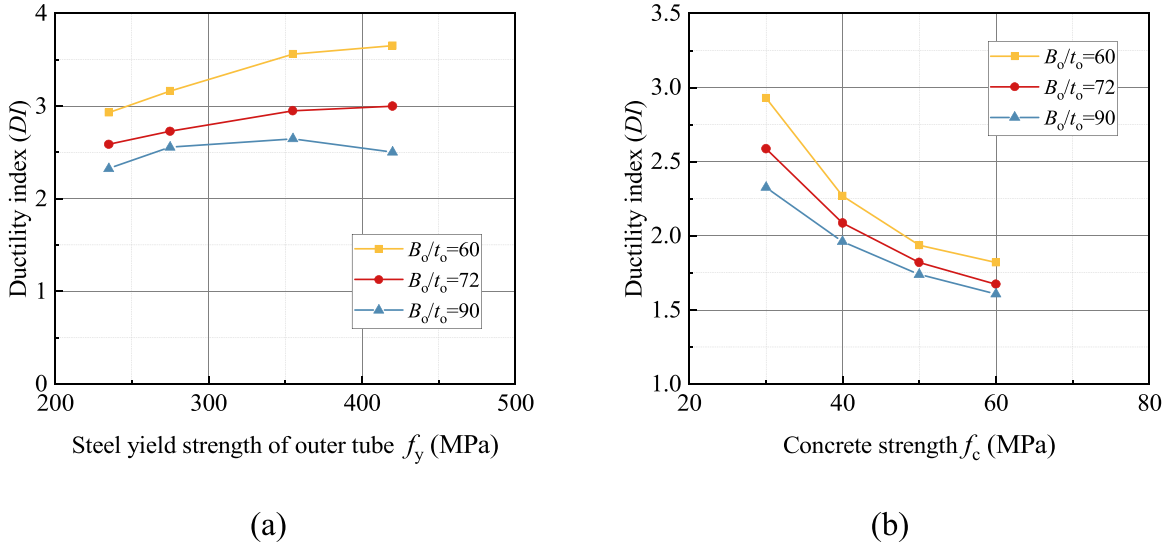

Fig. 19. Influence of (a) f_{yo} and (b) f_c on the ductility of CFDSST columns.

Table 5
Increase efficiency of f_{yo} and f_c in the resistance of CFDSST columns.

(a) f_{yo}

Specimen	B_o (mm)	t_o (mm)	f_{yo} (MPa)	$N_{ul,FE}$ (kN)	$\Delta N_{ul,FE}$ (%)	$\frac{\Delta N_{ul,FE}}{\Delta f_{yo}}$
C1	180	2	235	1434.6	-	-
C5	180	2	275	1487.1	0.04	0.21
C6	180	2	355	1631.9	0.14	0.27
C7	180	2	420	1762.2	0.23	0.29
C14	180	2.5	235	1531.7	-	-
C18	180	2.5	275	1617.9	0.06	0.33
C19	180	2.5	355	1789.5	0.17	0.33
C20	180	2.5	420	1948.7	0.27	0.35
C27	180	3	235	1627.4	-	-
C31	180	3	275	1736.2	0.07	0.39
C32	180	3	355	1933.6	0.19	0.37
C33	180	3	420	2123.3	0.30	0.39
C40	240	2	235	2265.1	-	-
C44	240	2	275	2348.5	0.04	0.22
C45	240	2	355	2560	0.13	0.25
C46	240	2	420	2649.8	0.17	0.22
C53	240	2.5	235	2449.3	-	-
C57	240	2.5	275	2560.1	0.05	0.27
C58	240	2.5	355	2787.4	0.14	0.27
C59	240	2.5	420	2949	0.20	0.26
C65	240	3	235	2558.6	-	-
C69	240	3	275	2691.8	0.05	0.31
C70	240	3	355	2960.8	0.16	0.31
C71	240	3	420	3185.3	0.24	0.31
C78	300	2	235	3288.8	-	-
C82	300	2	275	3440.8	0.05	0.27
C83	300	2	355	3580.5	0.09	0.17
C90	300	2.5	235	3392.9	-	-
C94	300	2.5	275	3486.6	0.03	0.16
C95	300	2.5	355	3633.9	0.07	0.14
C96	300	2.5	420	3742.6	0.08	0.10
C102	300	3	235	3711.2	-	-
C106	300	3	275	3873.6	0.04	0.26
C107	300	3	355	4200.2	0.13	0.26
C108	300	3	420	4465	0.20	0.26
C115	600	6	235	14,645	-	-
C119	600	6	275	15,299	0.04	0.26
C120	600	6	355	16,606	0.13	0.26
C121	600	6	420	17,669	0.21	0.26

(b) f_c

Specimen	B_o (mm)	t_o (mm)	f_c (MPa)	$N_{ul,FE}$ (kN)	$\Delta N_{ul,FE}$ (%)	$\frac{\Delta N_{ul,FE}}{\Delta f_c}$
C1	180	2	30	1434.6		
C2	180	2	40	1714.2	0.19	0.58
C3	180	2	50	2009.8	0.40	0.60
C4	180	2	60	2303.1	0.61	0.61
C14	180	2.5	30	1531.7	-	-
C15	180	2.5	40	1815.9	0.19	0.56
C16	180	2.5	50	2101.3	0.37	0.56
C17	180	2.5	60	2388.3	0.56	0.56
C27	180	3	30	1627.4	-	-
C28	180	3	40	1911.1	0.17	0.52
C29	180	3	50	2193.3	0.35	0.52
C30	180	3	60	2438.4	0.50	0.50
C40	240	2	30	2265.1	-	-
C41	240	2	40	2793.2	0.23	0.70
C42	240	2	50	3334	0.47	0.71
C43	240	2	60	3884.4	0.71	0.71
C53	240	2.5	30	2449.3	-	-
C54	240	2.5	40	2979.3	0.22	0.65
C55	240	2.5	50	3507.6	0.43	0.65
C56	240	2.5	60	4010.1	0.64	0.64
C65	240	3	30	2558.6	-	-
C66	240	3	40	3083	0.20	0.61
C67	240	3	50	3605.8	0.41	0.61
C68	240	3	60	4127.7	0.61	0.61
C78	300	2	30	3288.8	-	-
C79	300	2	40	3999.7	0.22	0.65
C80	300	2	50	4982.8	0.52	0.77
C81	300	2	60	5814.5	0.77	0.77
C90	300	2.5	30	3392.9	-	-
C91	300	2.5	40	4272.4	0.26	0.78
C92	300	2.5	50	5130.8	0.51	0.77
C93	300	2.5	60	5985.3	0.76	0.76
C102	300	3	30	3711.2	-	-
C103	300	3	40	4552.3	0.23	0.68
C104	300	3	50	5385.9	0.45	0.68
C105	300	3	60	6223.9	0.68	0.68
C115	600	6	30	14,645	-	-
C116	600	6	40	17,683	0.21	0.62
C117	600	6	50	20,720	0.41	0.62
C118	600	6	60	23,758	0.62	0.62

instead have methods for CFST cross-sections. Accordingly, the current section proposes a new expression to determine the axial load-bearing capacity of CFDSST short columns based on the specific properties of these members, including the stiffening effect and the significant influence of confinement on the concrete infill provided by the stiffened outer steel sections. Previous research has shown that size effects can be important for square columns, but are less significant for circular members [43]. Additionally, the size effects for CFDSST columns are more complicated owing to the presence of two steel tubes, and the stiffeners. Therefore, it is proposed that the strength of the confined concrete f_{cc} is determined using the expression given in Eq. (28), as proposed by Liang and Fragomeni [44], and the proposed resistance of CFDSST columns $N_{ul,Prop}$ is given by Eq. (29).

$$f_{cc} = \gamma_c f_c + k_1 f_{rp} \quad (f_{cc} \geq f_c) \tag{28}$$

$$N_{ul,Prop} = \rho A_{sq} f_{yo} + A_c f_{cc} + A_{si} f_{yi} + A_{ss} f_{ys} \tag{29}$$

In these expressions, γ_c is the strength reduction factor for the compressive strength that accounts for the size effect of the column and is defined by Eq. (30) according to Gao et al. [43]; f_{rp} is the lateral confining pressure on the concrete and is determined by Eq. (31) as proposed by Xu et al. [45]; and k_1 is a constant and is taken as 4.1.

$$\gamma_c = 1.85 D_c^{-0.135} \quad (0.85 \leq \gamma_c \leq 1.0) \quad , D_c = B_o - 2t_o \tag{30}$$

$$f_{rp} = 0.0194((B_o/2 - t_o)/t)^{-0.415} \times f_{yo} \tag{31}$$

7.5. Evaluation of design predictions

The various design expressions were applied to the columns examined in the parametric study. A comparison of the resulting design resistances with the $N_{ul,FE}$ and $N_{ul,Exp}$ values discussed earlier, is presented in Fig. 27 and Table 6. From Fig. 27(a), it is observed that the proposed model (indicated by the yellow dots) provides the most accurate predictions, and are within + /- 10% of the $N_{ul,FE}$ values. With reference to Fig. 27(b), the proposed model also provides better predictions for the experimental load capacities, where the majority of design values are within 10% of $N_{ul,\ FE.}$ From Table 6, it is observed that Eurocode 4 [26], BS5400 [27] and DBJ1315–2010 [28] generally underestimate the ultimate resistance of CFDSST columns by mean values of 15%, 15% and 7%, respectively. On the other hand, the proposed model provides more accurate predictions with mean and COV (coefficient of variation) $N_{ul,\ prop}/N_{ul,FE}$ values of 0.95 and 0.042, respectively. For the comparison of various design resistances with the capacities obtained by the test specimens, it is once again observed that Eurocode 4 [26], BS5400 [27] and DBJ1315–2010 [28] generally underestimate the ultimate resistance of the CFDSST columns, while the proposed model provides a more accurate prediction of the response with mean and COV $N_{ul,\ prop}/N_{ul,Exp}$ values of 0.95 and 0.076, respectively. The improved accuracy of the proposed method is owing to the consideration given to the two steel tubes, the stiffeners, the confinement provided to the infill concrete and the size effects.

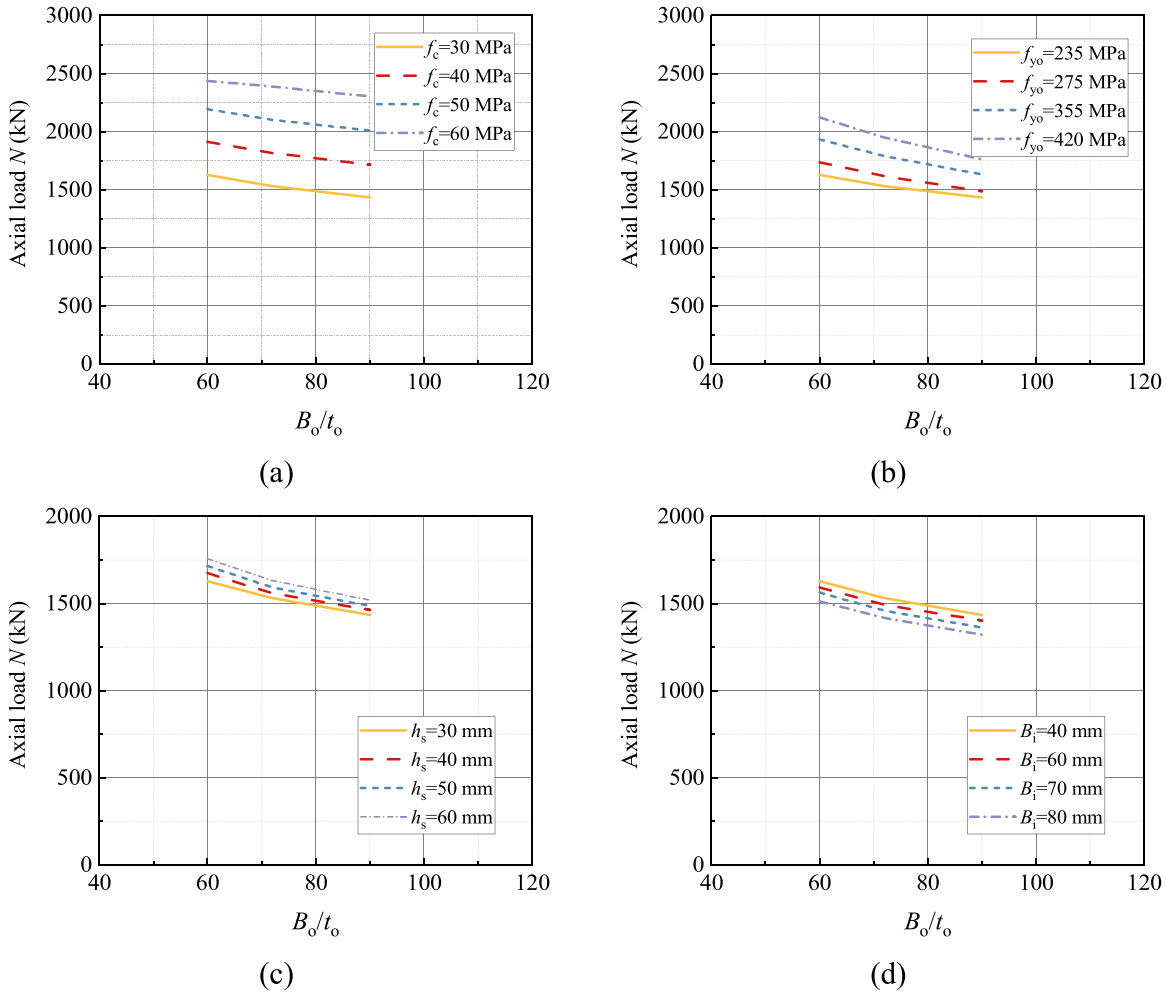

Fig. 21. Influence of B_o/t_o on the resistance of CFDSST columns with varying (a) concrete strength f_c, (b) outer tube yield strength f_{yo}, (c) stiffener depth h_s and (d) size of inner tube B_i.

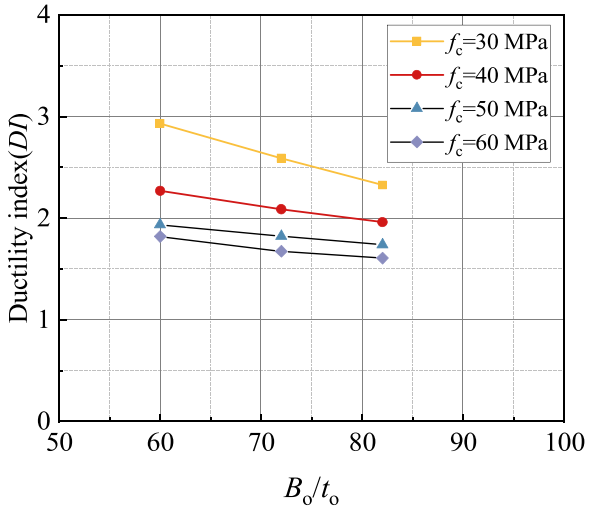

Fig. 22. Influence of B_o/t_o ratio on the ductility index DI of CFDSST columns.

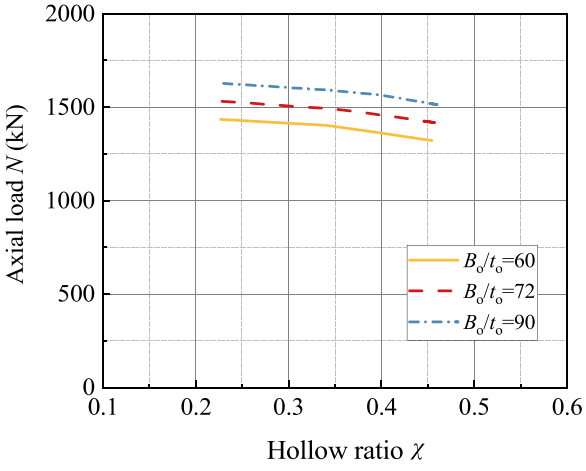

Fig. 23. Influence of χ on the load resistance of CFDSST columns.

To raise the confidence of the proposed design model, the reliability index (β) is further calculated to assess the security of the mentioned design methods. β is calculated as:

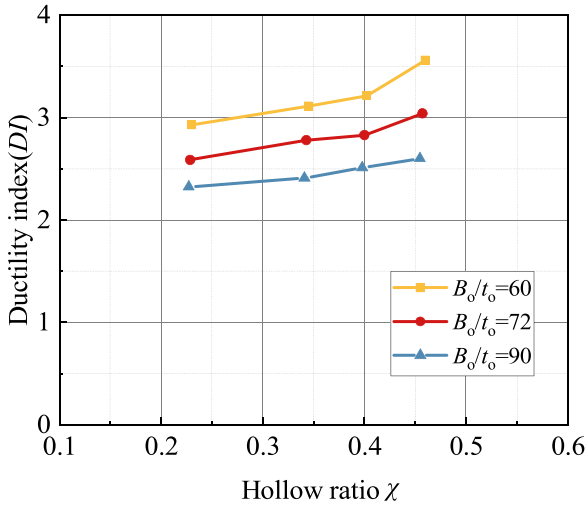

Fig. 24. Influence of χ on the ductility of CFDSST columns.

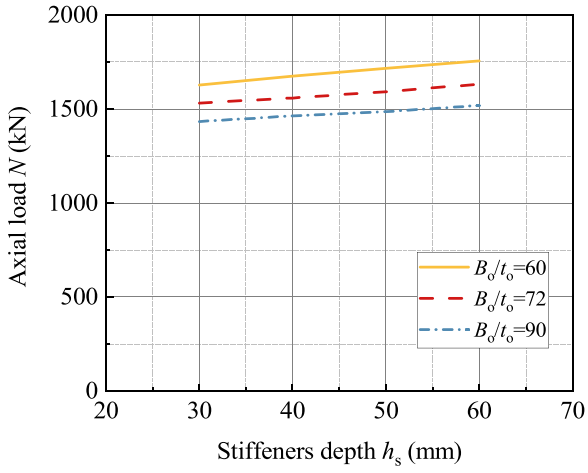

Fig. 25. Influence of h_s on the resistance of CFDSST columns.

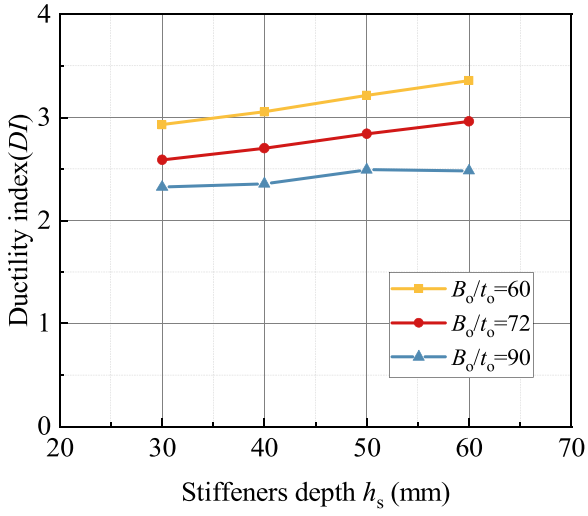

Fig. 26. Influence of on the h_s ratio ductility of CFDSST columns.

$$\beta = \frac{Ln\left(\frac{P \cdot M \cdot F}{\phi}\right)}{\alpha\sqrt{V_M^2 + V_P^2 + V_F^2}} \tag{32}$$

According to Lai and Varma [46], P is the average ration of $P_u/P_{u,code}$. The values of M and F, are taken as 1.10 and 1.0, respectively. The value of linearization approximation coefficient α is taken as 0.7 according to ASCE 7–16 [47]. V_M, V_F and V_P are the coefficients of variation of material, fabrications and P, respectively. 0.193 and 0.05 are suggested by Lai and Varma [46] for V_M and V_F, respectively. The strength reduction factor ϕ is equal to 0.75 following the recommendation of ANSI/AISC 360–16 [48]. The method for calculating the required parameters is consistent with the previous research [32,49]. The target reliability index is 2.5 for the purpose of avoiding sudden failure or wide-spread progression of damage [48]. As can be observed from Table 6, the proposed design has yielded a reliability index of 2.97 when compared to FE and test results, which confirms the reliability of this proposal.

8. Conclusions

This paper presents for the first time the results of a series of experiments on cold-formed concrete-filled double-skin steel stiffened tubular (CFDSST) columns under direct axial compression. This data is supplemented by a large database of results from numerical analyses, which was obtained using a newly developed finite element analysis model that was validated using the experimental data. A summary of the key findings is given as follows:

(1) A total of fifteen tests were conducted on short columns, including thirteen CFDSST cross-sections and two concrete-filled stiffened steel tubular (CFSST) members. All were tested under pure axial compression loading conditions. The results showed that replacing the core concrete of a CFSST column with a hollow inner steel tube produced columns with approximately similar ultimate axial strength but with greater ductility. Additionally, the CFDSST columns had higher post-peak load ultimate resistance compared with the CFSST columns. Additionally, it has been found that columns with relatively high χ values have lower self-weight and material usage requirements for the same B_o value, and therefore can provide an efficient structural solution.

(2) All of the test specimens failed by the local buckling of the outer steel tube together with concrete crushing after the attainment of the ultimate resistance. There was evidence of local buckling of the inner steel tube also. It is noteworthy that there was no evidence of steel fracture in the corner regions or near the welds, which highlights the good deformation capacity of the new CFDSST columns.

(3) Finite element (FE) models for the CFDSST columns were developed and validated through comparisons with the test data, and very good agreements were found.

(4) The validated FE model was employed to conduct a parametric study on CFDSST columns to understand their behaviour and evaluate their ultimate resistance with different geometric and material properties. The results showed that the ultimate resistance of CFDSST columns is significantly affected by the strength of the infill concrete and the ductility of CFDSST columns is improved for members with relatively lower B_o/t_o ratios, as well as relatively higher B_i/B_o ratios and yield strengths of the outer tube.

(5) In terms of the design expressions, it was found that the design resistance value predicted by Eurocode 4 [26], BS5400 [27] and DBJ1315-2010 [28] generally underestimates the ultimate resistance of CFDSST columns. A new design expression was proposed which provides much more accurate results because it accounts for the presence of the two steel tubes, the stiffeners in

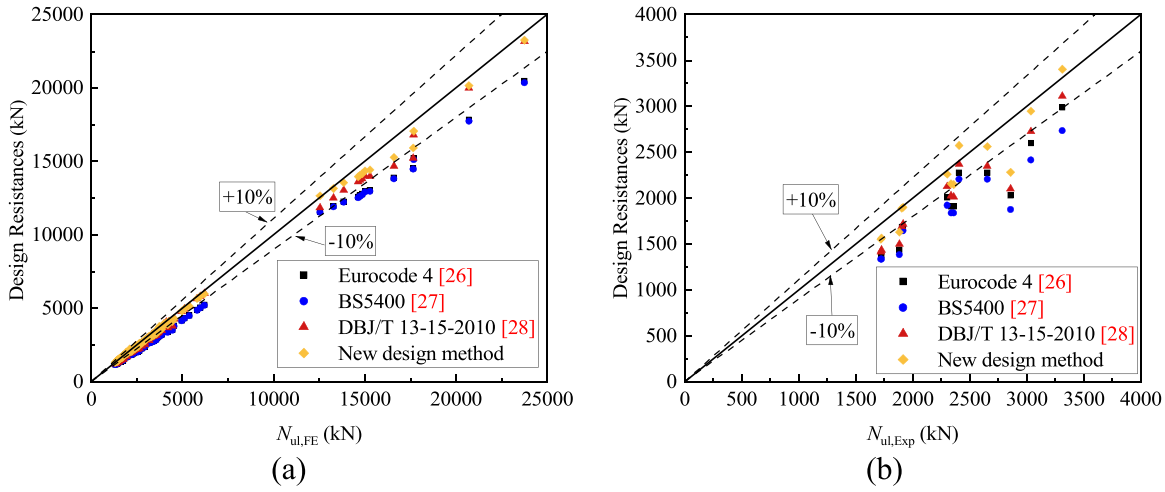

Fig. 27. Comparison of various design resistances with the capacities obtained by (a) finite element model and (b) experimental investigation.

Table 6
Statistical evaluation of comparison of various design resistances with the capacities obtained by the FE modelling/test specimens.

	EC4[26] $\frac{N_{ul,EC4}}{N_{ul,FE}}$	BS5400[27] $\frac{N_{ul,BS5400}}{N_{ul,FE}}$	DBJ1315-2010[28] $\frac{N_{ul,DBJ}}{N_{ul,FE}}$	Proposed model $\frac{N_{ul,prop}}{N_{ul,FE}}$
Comparison of various design resistances with the capacities obtained by the FE modelling				
Mean	0.85	0.85	0.93	0.96
COV	0.033	0.034	0.030	0.031
Max	0.92	0.92	1.00	1.05
Min	0.79	0.79	0.85	0.90
β	3.84	3.87	3.22	2.97
Comparison of various design resistances with the capacities obtained by the test specimens				
Mean	0.84	0.80	0.87	0.95
COV	0.075	0.081	0.075	0.076
Max	0.95	0.92	0.98	1.07
Min	0.71	0.66	0.73	0.80
β	3.77	4.01	3.52	2.96

the outer tube, the influence of the confinement provided to the infill concrete and also the size effects which affect square composite columns.

(6) Overall, these members were shown to provide very promising performance for high-load bearing applications, both in terms of load-carrying capacity and ductility, for less material usage than CFSSTs.

CRediT authorship contribution statement

Zhang JUN-HUA: Writing – original draft, Visualization, Methodology, Investigation, Data curation. **Hassanein M.F.:** Writing – review & editing, Visualization, Supervision, Project administration, Methodology, Formal analysis, Data curation, Conceptualization. **Cashell Katherine Ann:** Writing – review & editing, Visualization, Formal analysis, Data curation, Conceptualization. **HADZIMA-NYARKO MARIJANA:** Writing – review & editing, Visualization, Methodology, Data curation. **Zu Yang:** Writing – original draft, Visualization, Validation, Software, Investigation, Data curation. **Shao YONG-BO:** Supervision, Resources, Methodology, Investigation, Funding acquisition, Conceptualization.

Declaration of Competing Interest

The authors declare that they have no known competing financial interests or personal relationships that could have appeared to influence the work reported in this paper.

Data Availability

Data will be made available on request.

Acknowledgement

This study is supported by Scientific Innovation Group for Youths of Sichuan Province (No. 2019JDTD0017), and such support is appreciated greatly by the authors.

References

[1] Ho JCM, Dong CX. Improving strength, stiffness and ductility of CFDST columns by external confinement. Thin-Walled Struct 2014;Vol.75:18–29.
[2] Pagoulatou M, Sheehan T, Dai XH, Lam D. Finite element analysis on the capacity of circular concrete-filled double-skin steel tubular (CFDST) stub columns. Eng Struct 2014;Vol.72:102–12.
[3] Elchalakani M, Karrech A, Hassanein MF, Yang B. Plastic and yield slenderness limits for circular concrete filled tubes subjected to static pure bending. Thin-Walled Struct 2016;Vol.109:50–64.
[4] Zhao XL, Han LH. Double skin composite construction. Prog Struct Eng Mater 2006;Vol.8(3):93–102.
[5] Tao Z, Han LH, Zhao XL. Behaviour of concrete-filled double skin (CHS inner and CHS outer) steel tubular stub columns and beam-columns. J Constr Steel Res 2004; Vol. 60(8):1129–58.
[6] Huang H, Han LH, Zhao XL. Investigation on concrete filled double skin steel tubes (CFDSTs) under pure torsion. J Constr Steel Res 2013;Vol. 90:221–34.
[7] Guo Z, Chen Y, Wang Y, Jiang MY. Experimental study on square concrete-filled double skin steel tubular short columns. Thin-Walled Struct 2020;Vol. 156(0): 107017.
[8] Zhao XL, Grzebieta R. Strength and ductility of concrete filled double skin (SHS inner and SHS outer) tube. Thin-Walled Struct 2002;Vol.40(2):199–213.
[9] Zhao XL, Han B, Grzebieta RH. Plastic mechanism analysis of concretre-filled double-skin (SHS inner and SHS outer) stub columns. Thin-Walled Struct 2002; Vol.40(10):815–33.
[10] Hassanein MF, Elchalakani M, Karrech A, Patel VI, Yang B. Behaviour of concrete-filled double-skin short columns under comprssion through finite element modelling: SHS outer and SHS inner tubes. Structures 2018;Vol.14(1):358–75.
[11] Hassanein MF, Kharoob OF, Gardner L. Behaviour and design of square concrete-filled double skin tubular columns with inner circular tubes. Eng Struct 2015; Vol.100:410–24.
[12] Huang H, Han LH, Tao Z, Zhao XL. Analytical behaviour of concrete-filled double skin steel tubular (CFDST) stub columns. J Constr Steel Res 2010;Vol.66(4): 542–55.
[13] Han LH, Tao Z, Huang H, Zhao XL. Concrete-filled double skin (SHS outer and CHS inner) steel tubular beam-columns. Thin-Walled Struct 2004;Vol.42(9):1329–55.
[14] Zhao XL, Grzebieta RH, Elchalakani M. Test of concrete-filled double skin and (SHS outer CHS inner) composite stub columns. Adv Steel Struct 2002;Vol.1:567–74.
[15] Tao Z, Han LH, Wang ZB. Experimental behaviour of stiffened concrete-filled thin-walled hollow steel structural (HSS) stub columns. J Constr Steel Res 2005;Vol. 61 (7):962–83.

[16] Tao Z, Han LH, Wang DY. Experimental behaviour of concrete-filled stiffened thin-walled steel tubular columns. Thin-Walled Struct 2007;Vol. 45(5):517–27.
[17] Tao Z, Han LH, Wang D-Y. Strength and ductility of stiffened thin-walled hollows steel structural stub columns filled with concrete. Thin-Walled Struct 2008;Vol. 46 (10):1113–28.
[18] Liang W, Dong JF, Wang QY. Mechanical behaviour of concrete-filed double-skin steel tube (CFDST) with stiffeners under axial and eccentric loading. Thin-Walled Struct 2019;Vol. 138(5):215–30.
[19] Ding M, Shen L, Yang B. FE simulation of a new type of concrete-filled double skin steel tube with stiffeners under axial loading. Lect Notes Civ Eng 2021;Vol.101: 1725–35.
[20] Zhang YC, Chen Y. Experimental study and finite element analysis of square stub columns with straight ribs of concrete-filled thin-walled steel tube. J Build Struct 2006;Vol.5(27):16–22.
[21] Dabaon MA, EI-Boghdadi MH, Hassanein MF. Experimental investigation on concrete-filled stainless steel stiffened tubular stub columns. Eng Struct 2009; Vol.31(2):300–7.
[22] Dabaon M, EI-Koriby S, EI-Boghdadi M, Hassanein MF. Confinement effect of stiffened and unstiffened concrete-filled stainless steel tubular stub columns. J Constr Steel Res 2009;Vol. 65(8-9):1846–54.
[23] Wang ZB, Gao HY, Chi SY, Liao FY. Behaviour of concrete-filled double-skin thin-walled steel tubular columns under eccentric compression. J Build Struct 2018; Vol.5(39):124–31.
[24] Wang ZB, Zhang WA, Chi SY, Li YJ. Flexural behaviour of composite concrete-filled square thin-walled steel tubular specimens. J Build Struct 2017;Vol.7(38):78–84.
[25] Wang ZB, Guo JT, Gao HY, Chi SY, Yu X, Lin TW. Study on the behaviour of concrete-filled double-skin thin-walled steel tubular stub columns under axial compression. Prog Steel Build Struct 2018;Vol.2(20):53–9.
[26] Eurocode 4. BS EN 1994-1-1. Design of composite steel and concrete structures, Part1.1, General rules and 681rules for building, 682. London: British Standards Institution,; 2004.
[27] BS5400. Steel, Concrete and Composite Bridges, Part 5, Code of Practice for Design of Composite Bridges. London: British Standards Institution,; 1979. p. 684.
[28] DBJ/T 13-51-2010. Technical specification for concrete-filled steel tubular structures. 685Fuzhou (China). Constr Dep Fujian Prov 2003.
[29] Tao Z, Han LH, Wang ZB. Experimental behavior of stiffened concrete-filled thin-walled hollow steel structural (HSS) stub columns. J Constr Steel Res 2005;Vol. 61 (7):962–83.
[30] ASTM A370-2017. Standard Test Methods and Definitions for Mechanical Testing of Steel Products. Portland: American Society for Testing and Materials; 2017.
[31] GB/T 228.1-2010. Metallic Materials-Tensile Testing-Part 1: Method of test at Room Temperature. Beijing: Standards Press of China,; 2017.
[32] Rohola R, Hélder D C, Rui A S, Luís L, Aldina S. Buckling resistance of concrete-filled cold-formed steel (CF-CFS) built-up short columns under compression. Thin-Walled Struct 2022;Vol.170:0263–8231.
[33] Zhou Z, Gan D, Zhou XH. Improved composite effect of square concrete-filled steel tubes with diagonal binding ribs. J Struct Eng 2019;Vol. 145(10). pp. 4019112(1-12).
[34] Eurocode 3. Design of Steel Structures, Part4.4, Plate Elements Without Longitudinal 729 Stiffeners. London: British Standards Institution; 1997.
[35] ABAQUS. ABAQUS Standard User's Manual, Version 2020. Providence (RI, USA): Dassault Systèmes Corp; 2020.
[36] Liu JP, Zhou XH, Gan D. Effect of friction on axially loaded stub circular tubed columns. Adv Struct Eng 2016;Vol. 19(3):546–59.
[37] Ayough P, Ramli Sulong NH, Ibrahim Z. Analysis and review of concrete-filled double skin steel tubes under compression. Thin-Walled Struct 2020;Vol. 148: 106495.
[38] Tao Z, Uy B, Han LH, Wang ZB. Analysis and design of concrete-filled stiffened thin-walled steel tubular columns under axial compression. Thin-Walled Struct 2009;Vol. 47(12):1544–56.
[39] N. Abdel-Rahman, K.S. Sivakumaran, 1997, "Material properties models for analysis of cold-formed steel members", Vol. 123(9): 1135–1143.
[40] Tao Z, Wang ZB, Yu Q. Finite element modelling of concrete-filled steel stub columns under axial compression. J Constr Steel Res 2013;Vol. 89:121–31.
[41] Yu T, Teng JG, Wong YL, et al. Finite element modelling of confined concrete-I: drucker-prager type plasticity model. Eng Struct 2010;Vol. 32(3):665–79.
[42] Zhou F, Lama L, Zhao KZ. Design of stainless steel CHS-concrete infill-carbon steel CHS double-skin stub columns. Eng Struct 2023;Vol. 278:115479.
[43] Gao P, Zhou XH, Liu JP, Wang XD, Chen YF. Experimental assessment on the size effects of square concrete-filled steel tubular columns under axial compression. Eng Struct 2023;Vol. 281:115706.
[44] Liang QQ, Fragomeni S. Nonlinear analysis of circular concrete-filled steel tubular short columns under axial loading. J Constr Steel Res 2009;Vol. 65(12):2186–96.
[45] Xu Y, Shao YB, Hassanein MF, Silvestre N. Innovative compressive design resistance and behaviour of concrete-filled short columns with stiffened square steel sections. J Constr Steel Res 2022;Vol. 198:107510.
[46] Lai Z, Varma Amit H. High-strength rectangular CFT members: database, modeling, and design of short columns. J Struct Eng 2018;Vol. 144(5):04018036.
[47] ASCE. Minimum Design Loads for Buildings and Other Structures. Reston, VA: ASCE 7-10; 2017.
[48] AISC. Specification for Structural Steel Building. Chicago: AISC 360-16; 2016.
[49] Ayough P, Ibrahim Z, Sulong NHR, et al. Numerical analysis of square concrete-filled double skin steel tubular columns with rubberized concrete. Structures 2021; Vol. 32:1026–47.